



**HAL**  
open science

# Techno-economic analysis of production of bio-oil from catalytic pyrolysis of olive mill wastewater sludge with two different cooling mechanisms

Muhammad Shoaib Ahmed Khan, Najla Grioui, Kamel Halouani, Riad Benelmir

## ► To cite this version:

Muhammad Shoaib Ahmed Khan, Najla Grioui, Kamel Halouani, Riad Benelmir. Techno-economic analysis of production of bio-oil from catalytic pyrolysis of olive mill wastewater sludge with two different cooling mechanisms. *Energy Conversion and Management*: X, 2021, pp.100170. 10.1016/j.ecmx.2021.100170 . hal-03511910

**HAL Id: hal-03511910**

<https://hal.univ-lorraine.fr/hal-03511910v1>

Submitted on 22 Jul 2024

**HAL** is a multi-disciplinary open access archive for the deposit and dissemination of scientific research documents, whether they are published or not. The documents may come from teaching and research institutions in France or abroad, or from public or private research centers.

L'archive ouverte pluridisciplinaire **HAL**, est destinée au dépôt et à la diffusion de documents scientifiques de niveau recherche, publiés ou non, émanant des établissements d'enseignement et de recherche français ou étrangers, des laboratoires publics ou privés.



Distributed under a Creative Commons Attribution - NonCommercial 4.0 International License

# 1 **Techno-economic analysis of production of bio-oil from catalytic pyrolysis** 2 **of olive mill wastewater sludge with two different cooling mechanisms**

3  
4 Muhammad Shoaib Ahmed Khan<sup>a\*</sup>, Najla Grioui<sup>b,c</sup>, Kamel Halouani<sup>b,c</sup>, Riad Benelmir<sup>a</sup>  
5 <sup>a</sup>LERMAB, Faculty of Sciences and Technologies, Université de Lorraine, Vandoeuvre les  
6 Nancy, 54506, France

7 <sup>b</sup>Micro Electro Thermal Systems (UR13ES76), National Engineering School of Sfax,  
8 University of Sfax, IPEIS, Road Menzel Chaker km 0.5- PO Box 1172, 3018 Sfax, Tunisia

9 <sup>c</sup>Digital Research Center of Sfax, Technopole of Sfax, PO Box 275, Sakiet Ezzit, 3021 Sfax,  
10 Tunisia

## 11 **Abstract**

12  
13 A techno-economic analysis of production of bio-oil from catalytic pyrolysis of olive  
14 mill wastewater sludge has been performed with two different cooling schemes. The two  
15 configurations differ in the manner how the bio-oil vapors are quenched. In scheme-1, a  
16 vapor compression refrigeration machine is utilized for condensation of bio-oil vapors  
17 while in scheme-2, the vapor compression refrigeration machine is replaced by absorption  
18 refrigeration machine. The two schemes are modelled in Aspen Plus which provides mass  
19 and energy balances. For techno-economic analysis, Aspen process economic analyzer is  
20 employed. The model is first validated against experimental data from lab scale and then  
21 upscaled to an industrial scale of 100 tonnes/day wet biomass (93 tonnes/day dry biomass).  
22 Results show that the model with absorption refrigeration machine (scheme-2) has a  
23 slightly better process efficiency and a lower MFSP compared to the model with  
24 compression refrigeration machine (scheme-1). Total anticipated capital investment  
25 expenses for scheme-1 and scheme-2, comprising plant fixed capital investment (FCI),  
26 start-up, working capital, and interest, are expected to be €22.1 M and €17.5 M,  
27 respectively. The equipment costs are based on first quarter of 2021 and the economic life  
28 of the project is 20 years. Monte Carlo sensitivity analyses showed that the bio-oil MFSP is  
29 most vulnerable to discounted cash flow, income tax and bio-oil yield. The production cost

30 of bio-oil varies between €2.16/GGE and €6.19/GGE for scheme-1 and €1.78/GGE and  
31 €5.01/GGE for scheme-2 when cost parameters are varied within an industrially relevant  
32 range. The findings support the viability of producing bio-oil by catalytic fast pyrolysis on  
33 a commercial scale.

34 .

35 **Keywords:** Aspen Plus, Process simulation, Catalytic Fast pyrolysis, Fluidized bed, Olive  
36 mill wastewater sludge, Techno-economic study

37 \*Corresponding author: muhammad-shoaib-ahme.khan@univ-lorraine.fr

### 38 **1- Introduction**

39 The olive oil business is vital to the economies of various Mediterranean nations,  
40 including Spain, Greece, Turkey, Italy, and Tunisia. However, the extraction of olive oil  
41 produces a lot of olive mill wastewater (OMW), which is acidic in nature and pollutes the  
42 land and water. OMW is commonly disposed off in surrounding uninhabited places or lakes,  
43 where it remains for an extended period of time. Many procedures such as dilution, filtration,  
44 and sedimentation have been explored in the past to lessen the negative effects of OMW, but  
45 none of them seems to be effective. As a result, it became essential to apply a chemical  
46 method to transform it into certain innocuous yet valuable compounds [1]. These  
47 transformations can take place in two ways: biochemical and thermochemical [2].  
48 Torrefaction, pyrolysis, and gasification are the three basic types of thermochemical processes  
49 [3]. One of the possibilities of treating OMWS is the production of bio-oil through fast  
50 pyrolysis.

51 Under atmospheric pressure, fast pyrolysis is a thermal conversion process that  
52 transforms biomass into organic vapors, gases, water, and char in the absence of oxygen. The  
53 feedstock qualities are the primary determinants of product yield composition. At medium  
54 temperatures (about 400–500°C), fast pyrolysis of OMWS takes place. The organic vapor

55 portion, which is condensed into bio-oil, is the principal product. There is also the production  
56 of non-condensable gases, water, and biochar.

57 The main advantage of pyrolysis and combustion is that these processes shrink the  
58 large volumes of OMWS [1]. There are four types of pyrolysis in use: slow, intermediate, fast,  
59 and flash depending upon operating conditions. The most significant operating parameters  
60 which effect the product yields include heating rate, temperature of reactor, biomass particle  
61 size and residence time [5,6]. Intermediate pyrolysis (slow heating rates, intermediate solid  
62 residence times) is still in its infancy. Recent research has shown that intermediate pyrolysis  
63 oil derived from biomass and waste can provide a product oil with superior characteristics that  
64 is more comparable to biodiesel and diesel fuels [7]. Pyrolysis produces products in three  
65 different forms: solid (char), liquid (bio-oil), and syngas (pyrolytic gas); thus, it is widely used  
66 to convert biomass waste to energy [8]. Fast pyrolysis is regarded to be a suitable mechanism  
67 for generating clean and high energy content bio-oil from various types of biomass, among  
68 other thermochemical techniques [2]. In fast pyrolysis, biomass is heated to elevated  
69 temperature in a very limited time. The process is favorable if the bio-oil yield is maximum  
70 among other products. [9].

71 The use of the Aspen Plus modeling software in process modeling has grown in recent  
72 years. It is a modeling software that calculates a process's physicochemical and biological  
73 properties. The tool is popular because it may be used for all phases of the process (solid,  
74 liquid, and vapor) [10]. A few recent studies have shown that the simulation tool may be used  
75 to analyze pyrolysis experiments and forecast the process yields [11] . The tool is also useful  
76 for manipulating pyrolysis process parameters such as heating rate, temperature, solid  
77 residence time, feedstock size, and so on.

78 Many simulation studies on different types of biomass such as beachwood [12], empty  
79 fruit bench, sawdust and giant miscanthus [13], lignocellulosic feedstock [14], Napier grass

80 bagasse [15], pinewood [16], pine and forest residues [17], hybrid polar [18], spruce, wheat  
81 straw and corn stover [19] have been performed. In these simulation models, the biomass is  
82 decomposed into its basic building blocks (cellulose, hemicellulose and lignin) using *RYield*  
83 reactor, followed by kinetic reactions in *RCSTR* reactor and then finally secondary reactions  
84 in *RYield* reactor. The decomposition of biomass is governed by Power Law type reactions.

$$r = k * T^n * e^{-R/RT} \quad (1)$$

85 Where  $r$  is the rate of reaction,  $k$  is pre-exponential factor,  $T$  is the temperature,  $E$  is activation  
86 energy and  $R$  is gas law constant. These studies used the particle size distribution less than  
87 2mm and nitrogen was employed as fluidizing gas for pilot plant while non-condensable gases  
88 for industrial scale plants. Many researchers used catalyst ZSM-5 and sand as fluidized bed  
89 medium [12,20]. The temperature for pyrolysis reactor ranges from 400 to 520°C and bio-oil  
90 yield lies in the range of 28%- 64% [12,13,19]. The Aspen Plus model was effectively used to  
91 forecast pyrolysis product production and to study the effect of temperature on pyrolysis  
92 product output. So far, pyrolysis models which have been studied and developed in Aspen  
93 Plus are based on the work of Ranzi et. al. [21] which target the cellulosic biomass. In these  
94 studies, the simulation and experimental data were found to be in good agreement,  
95 demonstrating that Aspen Plus simulator may be used to forecast the yield of pyrolysis  
96 products. The simulation findings also showed that utilizing Aspen Plus, the pyrolysis  
97 operating parameters can be successfully adjusted, and the findings may be utilized for  
98 experimental testing.

99 The bio-oil derived from the pyrolysis is acidic in nature, has low energy content,  
100 contains oxygenated compounds and high viscosity [22]. Catalysts can be used to improve the  
101 characteristics of the bio-oil comparable to diesel. High-molecular-weight compounds are  
102 cracked into lower-molecular-weight products during the pyrolysis process. [23]. The  
103 catalytic pyrolysis bio-oil is thermally more stable and contains less acidic and oxygenated

104 compounds [24]. In the presence of catalysts, the distribution of pyrolysis products across the  
105 solid, liquid, and gaseous phases has been observed to change. Without additional  
106 upgradation, biomass catalytic pyrolysis produces useful biofuels such as gasoline and diesel  
107 fuel, heating oil, and other monocyclic aromatic hydrocarbons such as benzene, toluene, and  
108 xylene [25]. In general, two types of catalysts are utilized in pyrolysis, depending on the  
109 chemical nature of the material: acid and base catalysts. Biochar production is normally  
110 increased by acidic catalysts, whilst bio-oil production can be increased by base catalysts [26].  
111 The products distribution is highly dependent on the nature, quantity of catalyst, and operating  
112 conditions of the pyrolysis process [27].

113 Among the pyrolysis catalysts, zeolite-based catalysts are the most frequent. However, the  
114 generation of oxygenated molecules decreases while that of aromatic hydrocarbons increases  
115 [28]. Few studies have been published on the use of base catalysts in biomass pyrolysis. CaO,  
116 MGO, K<sub>2</sub>CO<sub>3</sub>, and Na<sub>2</sub>CO<sub>3</sub> are examples of metal oxides of alkali and alkaline that have  
117 shown the potential for catalytic pyrolysis, producing bio-oil with high heating value and  
118 lower oxygen compounds [29].

119 The catalysts used in pyrolysis may be classified into three types depending on the method  
120 utilized. In the first category, catalyst is mixed with biomass before entering the pyrolysis  
121 reactor. The second category deals with the catalyst already placed in the reactor and biomass  
122 added after thus making a direct contact. The catalysts for the third category are put into a  
123 second reactor, which is placed downstream of the primary reactor. In a study carried out by  
124 Dong et. al. [30], the researchers reported a three times more carbon product from two stage  
125 catalytic pyrolysis in the presence of light olefins than single stage reactor.

126 Several previous studies report the cost of producing bio-oil via fast  
127 pyrolysis [15,17,20,31–34] by varying assumptions for biomass cost, plant capacity, reactor  
128 technology, and other variables. Economic analysis of large-scale models was conducted in

129 Aspen Process Economic Analyzer (APEA) [19]. These studies have estimated the cost of  
130 bio-oil to range between €1.75 and €8.67/GGE (€0.014/MJ - €0.07/MJ). Capital cost for the  
131 study conducted by Wright et. al. [33] is €166 million for a pyrolysis plant of 2000  
132 tons/day. The economic analysis of a plant of 49 kg/hr Napier grass bagasse indicates that  
133 the capital cost is estimated to be €1.77 million and operating cost €0.25 million [15].

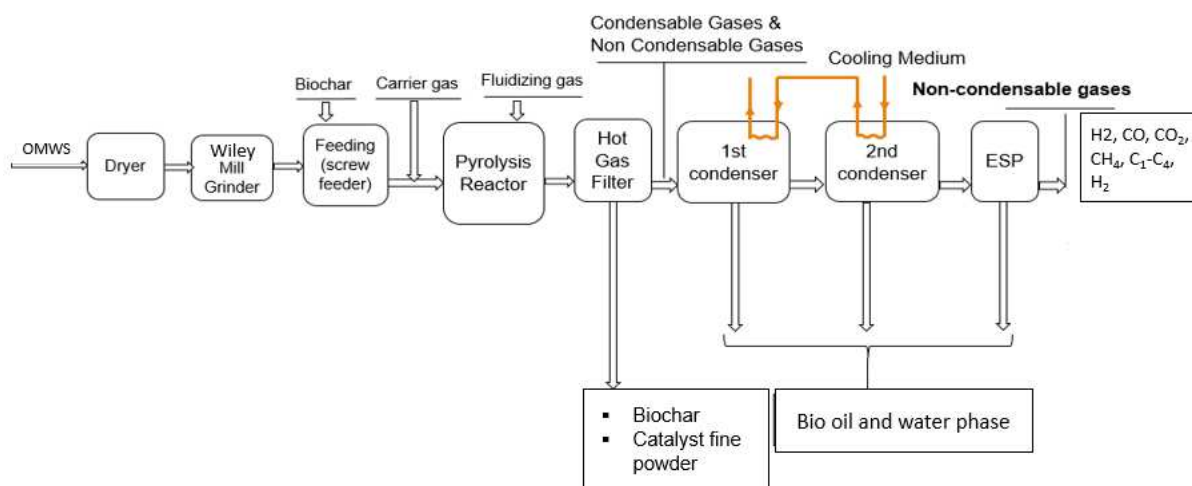
134 In this study, we propose to develop an Aspen Plus model which takes into account the  
135 global kinetic parameters for the production of pyrolytic bio-oil from fast pyrolysis of  
136 OMWS (catalytic and non-catalytic) and compare the simulation results with the  
137 experimental data of Agblevor et. al. [35]. After validation of results, the model is upscaled  
138 to commercial scale of 100 tonnes/day and two schemes are proposed. The schemes differ  
139 in the way of condensing the bio-oil vapors. In scheme-1, the bio-oil vapors are condensed  
140 using a compression refrigeration machine, while in scheme-2, an absorption cooling  
141 machine is employed for condensation. Finally, a techno-economic analysis is performed to  
142 assess the performance of both schemes on the basis of minimum fuel selling price (MFSP)  
143 of bio-oil.

## 144 **2- Materials and Methods**

### 145 *2.1- Experimental data*

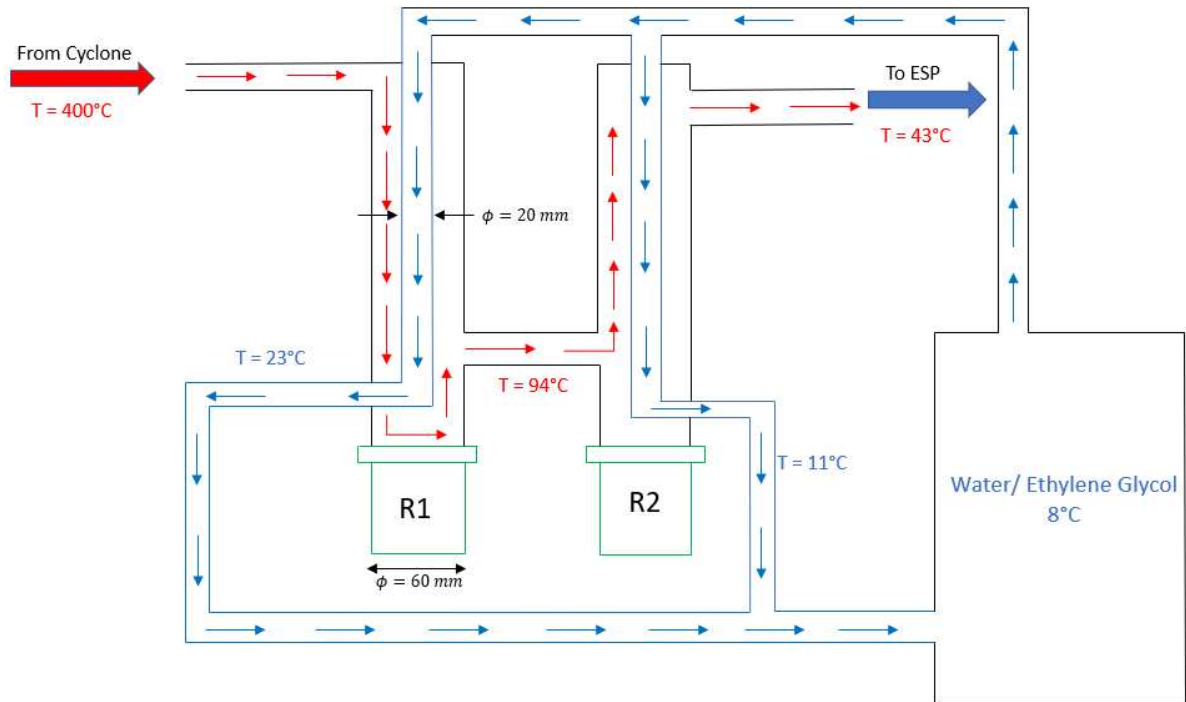
146 Experiments were performed by Agblevor et. al. [35] in Utah State University. Olive mill  
147 wastewater sludge (OMWS) was collected from a Tunisian evaporation pond. It is dried at  
148 ambient temperature before being ground to a size of around 2 mm. The 160 grams of ground  
149 biomass are mixed with 40 grams biochar to make it less sticky. Nitrogen gas at 25°C, 1.01  
150 bar is used as carrier to blow it into the fluidizing bed reactor. The fluidized bed reactor has a  
151 diameter of 50 mm and a length of 500 mm. The mixture of ground biomass, biochar and  
152 nitrogen is introduced into the pyrolysis reactor at ambient temperature. Nitrogen as fluidizing

153 gas enters from bottom of pyrolysis reactor at 300°C, 1.02 bar. Catalyst; red mud, is heated at  
 154 550°C for five hours before using it in the reactor. The experiment is performed at three  
 155 different temperatures i.e. 400, 450 and 500°C. Bio-oil, steam and biogas are gaseous  
 156 products while biochar and red mud are solid products. These are separated in a cyclone kept  
 157 at 400°C so that bio-oil may not condense at this stage. The gaseous products are then passed  
 158 through condensers (the first co-flow and the second counter-flow) to condense the bio-oil  
 159 and water vapors. Water/ethylene glycol mixture at 8°C was used as cold fluid in the  
 160 condensers (Fig. 2). Bio-oil aerosols, biogas and nitrogen are passed through electrostatic  
 161 precipitator (ESP) where bio-oil is collected at ambient temperature. The biogas and nitrogen  
 162 are non-condensable at ambient temperature and pressure and can be used for other purposes.



163 **Figure 1.** Schematic diagram of pyrolysis of OMWS





164

165

**Figure 2.** Schematic diagram of shell and tube heat exchanger

166

167 Proximate and ultimate analyses of OMWS and biochar are shown in the following Table 1.

168 **Table 1.** OMWS and biochar attributes [8]

Attribute	OMWS Biomass	OMWS Biochar
<i>Proximate analysis (wt. %)</i>		
Moisture	4.08	2.62
Fixed Carbon	22.21	25.43
Volatile Matter	64.43	33.42
Ash	13.36	41.15
<i>Ultimate analysis (wt. %)</i>		
Carbon	52.89	48.09
Hydrogen	7.16	4.69
Nitrogen	1.96	2.01
Sulfur	0.6	0.15
Oxygen	24.03	3.91
HHV (MJ/kg)	25.64	21.34

169

170 Catalyst red mud was used for catalytic pyrolysis while sand was used for non-catalytic

171 pyrolysis. The composition of red mud is given in the following Table 2.

172 **Table 2.** Red Mud composition [8]

Metal Oxide	wt. (%)
Fe <sub>2</sub> O <sub>3</sub>	13.36

Al <sub>2</sub> O <sub>3</sub>	52.89
SiO <sub>2</sub>	7.16
CaO	1.96
TiO <sub>2</sub>	0.6
Na <sub>2</sub> O	24.03

---

173

174 *2.2- Simulation model*

175 *2.2.1- Pilot scale*

176 Aspen Plus is a comprehensive powerful tool used by engineers and researchers for  
 177 a variety of applications including chemical processes, power generation, polymerization,  
 178 distillation, pharmaceuticals and fertilizers. It contains several tools to calculate mass and  
 179 energy balance, chemical equilibrium, reaction kinetics and perform optimization studies.  
 180 Users can benefit from extensive databases thermodynamic models and physical properties  
 181 to develop complicated and comprehensive processes. Its strength lies in the handling of  
 182 conventional and non-conventional solids, liquid and gas fuels [36]. Aspen Plus has been  
 183 used by many researchers for pyrolysis of biomass [37–40].

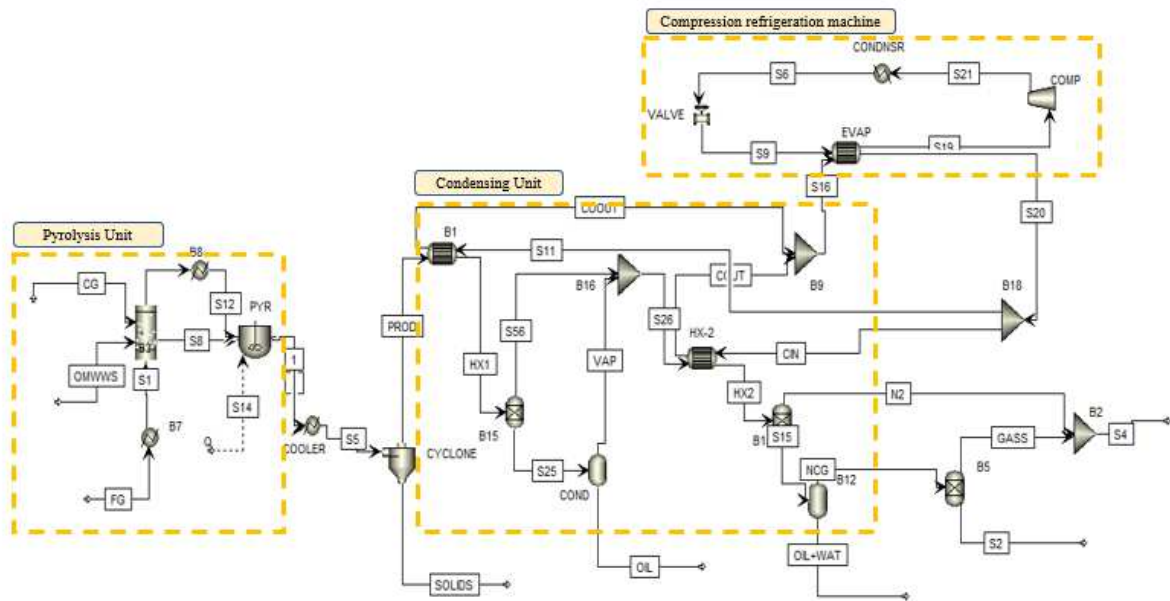
184 Components in Aspen Plus are divided into two categories: conventional and non-  
 185 conventional. The molecular structure of conventional components is known, and they may  
 186 be found in numerous Aspen Plus databanks. Because non-conventional components lack a  
 187 molecular formula, proximate and ultimate analyses are used to represent them [38].

188 In this work, catalytic and non-catalytic pyrolysis of OMWS is modelled using  
 189 ASPEN Plus ® software as shown in Figure 3. OMWS and biochar are defined as non-  
 190 conventional components and described on the basis of proximate and ultimate analysis  
 191 (Table 1). OMWS, biochar carrier gas and fluidization gas are fed into the fluidized bed  
 192 reactor where dehydration takes place. After dehydration, feedstock is fed into *RCSTR (PYR)*

193 reactor where biomass is disintegrated into bio-oil, biochar, water and gases according to the  
 194 global reaction equation (2).

$$OMWS = Bio\ oil + Biochar + Biogas + Water \quad (2)$$

195 The products exiting the reactor are cooled to 400°C using a simple cooler exchanger  
 196 (Heater) to keep the products at same temperature as cyclone. Biochar and catalyst are  
 197 separated in a cyclone and the gaseous products are passed through a first condenser (co-flow  
 198 HeatX) and cooled to 96°C. The products pass through two separators where bio-oil is  
 199 separated. About 70% of bio-oil is condensed in the first condenser. The remaining products  
 200 pass through a second condenser (counter-flow HeatX) and the temperature is further reduced  
 201 to 42°C. The products pass through two separators where bio-oil and water are separated from  
 202 the NCG.



203  
 204 **Figure 3.** Aspen Plus flowsheet of catalytic fast pyrolysis process of OMWS.

205 A list of Aspen Plus units and their description is given in Table 3.

206 **Table 3.** Aspen Plus unit models

Unit	Description
Fluidized bed reactor	Models the fluidization dynamics and calculates the minimum fluidization velocity and superficial velocity.

RCSTR	Stands for continuous stirred tank reactor. This unit is useful when kinetics of the chemical reaction are known.
Cyclone	Separates solids from gases
HX	Models shell and tube heat exchanger to heat or cool down inlet streams
Comp	Compressor used in compression refrigeration system
Flash2	Executes vapor-liquid equilibrium calculations
Sep	Separates inlet stream components into multiple outlet streams depending upon split fractions or specified flows

---

207

### 208 2.2.2- Specific heat capacity of non-conventional components

209 Based on the generic enthalpy model for coal, the special property techniques for  
 210 enthalpy and density for wood were chosen. The HCOALGEN technique, which is based on  
 211 ultimate and proximal analysis, was used to compute the OMWS enthalpy. The Kirov  
 212 correlation uses the proximate analysis to compute the heat capacity of biomass:

$$C_{p,j} = \sum_{j=1}^{ncn} w_j C_{p,ij} \quad (3)$$

213 where  $w_j$  is the mass fraction of the  $j$ th constituent on a dry basis,  $C_p$  is the heat capacity,  $i$  is  
 214 the component index,  $j$  is the constituent index. Each proximate analysis' temperature-  
 215 dependent heat capacity is taken into consideration using the equation below:

$$C_{p,ij} = a_{ij1} + a_{ij2}T + a_{ij3}T^2 + a_{ij4}T^3 \quad (4)$$

216 where 'a' is a parameter or element,  $i$  is the component index, and  $n$  is the constituent index (1  
 217 = moisture, 2 = FC, 3 = main VM, 4 = secondary VM, 5 = ash). The heat of combustion is  
 218 used to calculate the standard heat of formation. The char enthalpy was estimated using the  
 219 identical enthalpy and density procedures as for biomass, with the difference that instead of a  
 220 manual specification, the heat of combustion was computed using the Boie correlation (5):

$$\Delta_{C2} h_i^{dm} = [a_{1i}w_{C,i} + a_{2i}w_{H,i} + a_{3i}w_{S,i} + a_{4i}w_{O,i} + a_{5i}w_{N,i}]10^2 + a_{6i} \quad (5)$$

221 where  $w$  is the mass fraction of components  $C$  (carbon),  $H$  (hydrogen),  $S$  (sulfur),  $O$  (oxygen),  
222 and  $N$  (nitrogen). For parameters 1–6, default settings were utilized, which may be found in  
223 the Aspen Plus user manuals.

### 224 2.2.3- Physical property method

225 In order to get results that are as accurate and realistic as feasible, modeling  
226 procedures necessitate a careful selection of thermodynamic property method. As a result,  
227 choosing a property approach was one of the most important aspects of this research. A  
228 simulation engine's physical property methods are routines and equations for computing the  
229 thermodynamic and transport characteristics of material flows. The simulation can use  
230 physical property algorithms to interpret component behavior under various scenarios.  
231 Property methods are determined depending on the simulated circumstances and components.  
232 Because of the existence of hydrocarbons and light gases, the *RK-SOAVE* property method is  
233 used as the global thermodynamic model [36]. *RK-SOAVE* is comparable with *PENG-ROB*  
234 but it already contains a number of binary parameters for vapor-liquid and liquid-liquid  
235 equilibrium while *PENG-ROB* lacks these parameters. Thermal properties such as enthalpy,  
236 density and specific heat are determined from built-in models *HCOALGEN* and *DCHARIGT*  
237 in Aspen Plus. The enthalpy of non-conventional component is calculated as

$$H^S = \Delta_f h^S + \int_{T^{ref}}^T C_p^S dT \quad (6)$$

238 As molecular formula of the non-conventional component is unknown so  $\Delta_f h^S$  cannot  
239 be calculated directly. It is possible to calculate heat of formation from heat of combustion as  
240 combustion products and their molecular structures are well-known:

$$\Delta_f h^S = \Delta_c h^S + \Delta_f h_{cp}^S \quad (7)$$

241  $\Delta_f h_{cp}^S$  is the sum of the heats of formation of the combustion products multiplied by the mass  
242 fractions of the respective elements in the non-conventional component. Coal enthalpy model

243 *HCOALGEN* employs this approach to calculate the enthalpy of non-conventional  
244 components. *DCHARIGT* model is based on equations from IGT [41] and calculates density  
245 of char on dry basis using ultimate and sulfur analyses. As both conventional and non-  
246 conventional solids are involved in the simulation model, stream class *MCINCPSD* is a  
247 suitable choice. Molecular weights and other thermos-physical properties are retrieved from  
248 NIST database.

249 Aspen plus is flexible enough to integrate other programs like Fortran user-subroutines  
250 or Matlab. This feature is intended to model highly complex reactor models which otherwise  
251 cannot be used in predefined blocks in Aspen Plus.

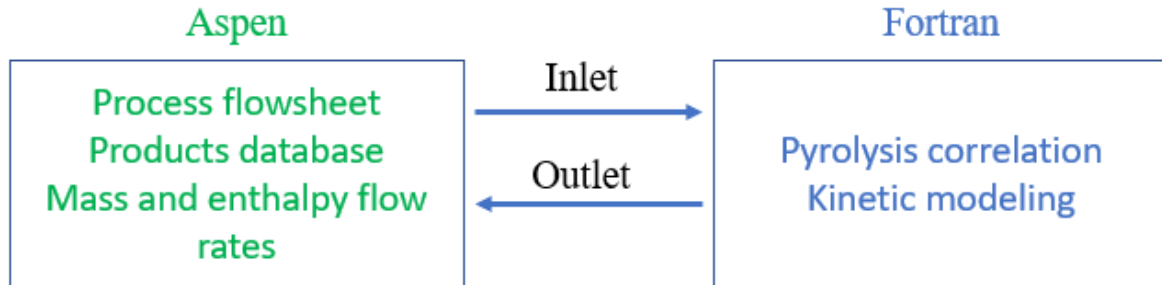
252 The kinetic reactions of pyrolysis are written in a separate Fortran file and then  
253 compiled using an intel compiler. The external Fortran user-subroutine is then coupled with  
254 Aspen Plus using a *dll* file. This method of coupling is different from the Fortran calculator  
255 blocks already embedded in Aspen Plus. Reactor inputs e.g. mass flow rate, temperature,  
256 volume etc. are transferred to Fortran file where chemical reactions take place by using  
257 empirical correlations and products are formed as a function of temperature. The results are  
258 sent back to Aspen Plus and can be seen in the output tab of the reactor.

#### 259 2.2.4- Pyrolysis section

260 For present study, fluidized bed reactor is 500 mm long and 50 mm in diameter with 100  
261  $\mu\text{m}$  orifice diameter of gas distributor. 160 grams of OMWS, 40 grams of biochar, 5 l/min of  
262 carrier gas (Nitrogen) and 13.3 l/min of fluidization gas (Nitrogen) are fed into the reactor.  
263 The residence time of the vapors is 2 seconds.

264 Two Aspen plus unit operations, the fluidized bed reactor (FBR) and pyrolysis reactor  
265 (*RCSTR*) are used to represent the pyrolysis section. The fluidized bed mimics the fluidization  
266 model of solids and calculates the minimum fluidization velocity. The *RCSTR* reactor  
267 represents the pyrolysis reactor where biomass is converted into pyrolysis products. Template

268 for reaction kinetics is unable to deal with the kinetics of equations (8) and (9), so kinetic  
 269 equations for OMWS pyrolysis are written in an external Fortran user-subroutine and then  
 270 linked with *RCSTR* reactor (Figure 4). A general reaction is given by equation (2).



271

272 **Figure 4.** Coupling of external user-subroutine with Aspen plus.

273

274 The reaction rate of the pyrolysis of OMWS is determined from the analysis of  
 275 experimental data of Agblevor et. al. [35] and formulated according to the modified Arrhenus  
 276 law proposed by Diaz and Broun [42].

$$R = k \cdot C_{k0} \cdot \left(\frac{F_k}{F_{k0}}\right)^n \quad (8)$$

277 where  $R$ ,  $k$ ,  $C_{k0}$ ,  $F_k$ ,  $F_{k0}$  and  $n$  are reaction rate (kg/m<sup>3</sup>.s), rate constant (1/s), concentration of  
 278 OMWS (kg/m<sup>3</sup>), remaining mass flow (kg/s), initial mass flow of OMWS (kg/s) and Order of  
 279 reaction ( $n=1$ ) respectively. The rate constant can be written by the following equation:

$$k = A \exp\left(\frac{E_a}{RT}\right) \quad (9)$$

280 where  $A$  is pre-exponential factor ( $A= 2.55 \times 10^4 \text{ s}^{-1}$ ),  $E_a$  is Activation Energy ( $E_a =$   
 281  $69.56 \text{ kJ/mol/K}$ ),  $T$  is temperature (K) and  $R$  is gas constant (J/mol. K). The subsequent  
 282 production of bio-oil, biochar, NCG and water is calculated by the following relation [42,43] .

$$R_i = f_i \times R \quad (10)$$

283 where:

284  $R_i$  = reaction rate of  $i$ -th product, kg of  $i$ -th product/m<sup>3</sup>.s

285  $f_i$  = stoichiometric factor of  $i$ -th product, kg of  $i$ -th product/kg of OMWS

286  $f_i$  used in this model is based on the experimental data at 400°C, 450°C and 500°C and given  
 287 in the following Table 4.

288 **Table 4.**  $f_i$  determined from experimental data of Agblevor et al. [8] and used in the model.

Component	$f_i$	$f_i$	$f_i$
	(kg/kg of OMWS) 400°C	(kg/kg of OMWS) 450°C	(kg/kg of OMWS) 500°C
CHAR	0.291	0.227	0.204
H <sub>2</sub> O	0.113	0.175	0.118
H <sub>2</sub>	0.005375	0.0114	0.01486
CO	0.01485	0.02205	0.045003
CO <sub>2</sub>	0.196	0.21765	0.252972
CH <sub>4</sub>	0.004	0.0078	0.014554
C <sub>2</sub> H <sub>6</sub>	0.0125	0.0162	0.02267
C <sub>3</sub> H <sub>8</sub>	0.0125	0.0162	0.02298
C <sub>4</sub> H <sub>10</sub>	0.00475	0.0087	0.009958
Bio-oil	0.346	0.298	0.295

289

#### 290 2.2.5- Condensers

291 Shell and tube heat exchangers were used to model the condensers in Aspen Plus. The  
 292 diameter of the shell is 60 mm and tube length is 500 mm with 20 mm diameter (Figure 2).  
 293 Water/ethylene glycol mixture is used as cooling medium at 8°C with flow rate of 8 kg/hr in  
 294 each heat exchanger. The components used in the simulation model are summarized in Table  
 295 5.

296 **Table 5.** List of components

Component ID	Type	Component Name	Alias
OMWS	Nonconventional		
CHAR	Nonconventional		
Ash	Nonconventional		
N <sub>2</sub>	Conventional	NITROGEN	N <sub>2</sub>
O <sub>2</sub>	Conventional	OXYGEN	O <sub>2</sub>
H <sub>2</sub>	Conventional	HYDROGEN	H <sub>2</sub>

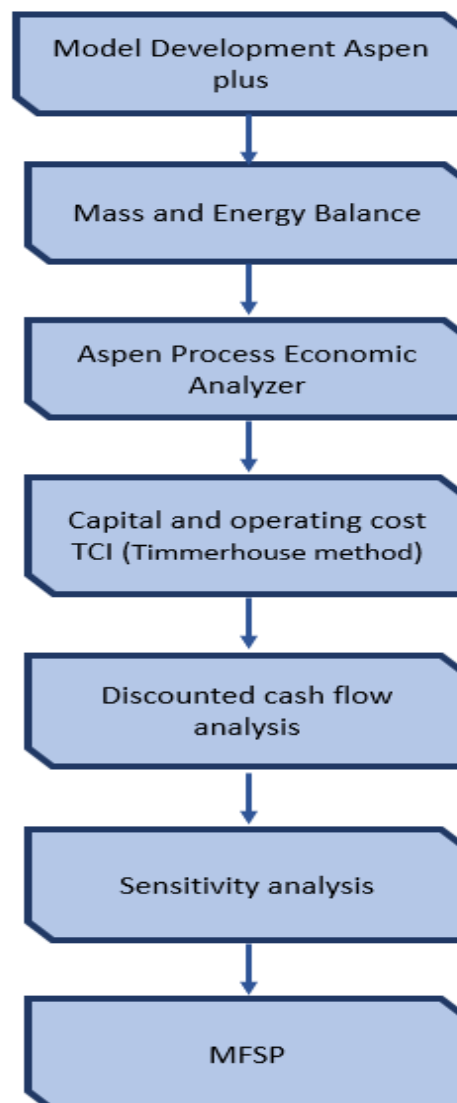


H <sub>2</sub> O	Conventional	WATER	H <sub>2</sub> O
CO	Conventional	CARBON-MONOXIDE	CO
CO <sub>2</sub>	Conventional	CARBON-DIOXIDE	CO <sub>2</sub>
CH <sub>4</sub>	Conventional	METHANE	CH <sub>4</sub>
C <sub>2</sub> H <sub>6</sub>	Conventional	ETHANE	C <sub>2</sub> H <sub>6</sub>
C <sub>3</sub> H <sub>8</sub>	Conventional	PROPANE	C <sub>3</sub> H <sub>8</sub>
C <sub>4</sub> H <sub>10</sub>	Conventional	ISOBUTANE	C <sub>4</sub> H <sub>10-2</sub>
Fe <sub>2</sub> O <sub>3</sub>	Solid	HEMATITE	Fe <sub>2</sub> O <sub>3</sub>
		ALUMINIUM-OXIDE-ALPHA-	
Al <sub>2</sub> O <sub>3</sub>	Solid	CORUNDUM	Al <sub>2</sub> O <sub>3</sub>
SiO <sub>2</sub>	Solid	SILICON-DIOXIDE	SiO <sub>2</sub>
TiO <sub>2</sub>	Solid	TITANIUM-DIOXIDE-RUTILE	TiO <sub>2</sub>
Na <sub>2</sub> O	Solid	SODIUM-OXIDE	Na <sub>2</sub> O
CaO	Solid	CALCIUM-OXIDE	CaO
ETHYL-01	Conventional	ETHYLENE-GLYCOL	C <sub>2</sub> H <sub>6</sub> O <sub>2</sub>
R22	Conventional	CHLORODIFLUOROMETHANE	CHClF <sub>2</sub>
Catalytic Bio-oil			
1-DECENE	Conventional	1-DECENE	C <sub>10</sub> H <sub>20-5</sub>
P-CRESOL	Conventional	P-CRESOL	C <sub>7</sub> H <sub>8</sub> O-5
1-UNDECE	Conventional	1-UNDECENE	C <sub>11</sub> H <sub>22-2</sub>
N-UNDECA	Conventional	N-UNDECANE	C <sub>11</sub> H <sub>24</sub>
4-ETHPHE	Conventional	P-ETHYLPHENOL	C <sub>8</sub> H <sub>10</sub> O-3
2-DODECA	Conventional	DECYL-METHYL-KETONE	C <sub>12</sub> H <sub>24</sub> O-N9
1-TRIDEC	Conventional	1-TRIDECENE	C <sub>13</sub> H <sub>26-2</sub>
N-TRIDEC	Conventional	1-TRIDECANOL	C <sub>13</sub> H <sub>28</sub> O
HEXADECA	Conventional	N-HEXADECANE	C <sub>16</sub> H <sub>34</sub>
1-TETRAD	Conventional	1-TETRADECENE	C <sub>14</sub> H <sub>28-2</sub>
TETRADEC	Conventional	N-TETRADECANE	C <sub>14</sub> H <sub>30</sub>
N-PENTAD	Conventional	1-PENTADECANOL	C <sub>15</sub> H <sub>32</sub> O
HEPTADEC	Conventional	N-HEPTADECANE	C <sub>17</sub> H <sub>36</sub>
1-HEPTAD	Conventional	1-HEPTADECENE	C <sub>17</sub> H <sub>34</sub> -D1
1-NON-DE	Conventional	1-NONADECANOL	C <sub>19</sub> H <sub>40</sub> O
PALMI-01	Conventional	PALMITONITRILE	C <sub>16</sub> H <sub>31</sub> N
TRICY-01	Conventional	TRICYCLOHEXYLAMINE	C <sub>18</sub> H <sub>33</sub> N
ETHYL-01	Conventional	ETHYL-OLEATE	C <sub>20</sub> H <sub>38</sub> O <sub>2</sub> -N1
BUTYL-01	Conventional	BUTYL-OLEATE	C <sub>22</sub> H <sub>42</sub> O <sub>2</sub> -N5
9-HEP-01	Conventional	9-HEPTADECANONE	C <sub>17</sub> H <sub>34</sub> O
Non-Catalytic bio-oil			
N-PEN-01	Conventional	N-PENTADECANE	C <sub>15</sub> H <sub>32</sub>
8-HEP-01	Conventional	8-HEPTADECENE	C <sub>17</sub> H <sub>34</sub> -N4
1-HEP-01	Conventional	1-HEPTADECENE	C <sub>17</sub> H <sub>34</sub> -D1
N-HEP-01	Conventional	N-HEPTADECANE	C <sub>17</sub> H <sub>36</sub>
N-HEX-01	Conventional	N-HEXADECANOIC-ACID	C <sub>16</sub> H <sub>32</sub> O <sub>2</sub>
METHY-01	Conventional	METHYL-PALMITATE	C <sub>17</sub> H <sub>34</sub> O <sub>2</sub> -N1
METHY-02	Conventional	METHYL-OLEATE	C <sub>19</sub> H <sub>36</sub> O <sub>2</sub>
OLEIC-01	Conventional	OLEIC-ACID	C <sub>18</sub> H <sub>34</sub> O <sub>2</sub>

297

298 *2.3- Industrial scale*

299 A simulation model of a hypothetical plant of 100 tonnes/day wet OMWS (93 tonnes/day  
300 dry OMWS) capacity is developed. The overall technique used in this analysis is depicted in  
301 Figure 5. Modeling, equipment size and costing, profitability analysis using the discounted  
302 cash flow (DCF) approach, and sensitivity analysis are all part of the methodology.



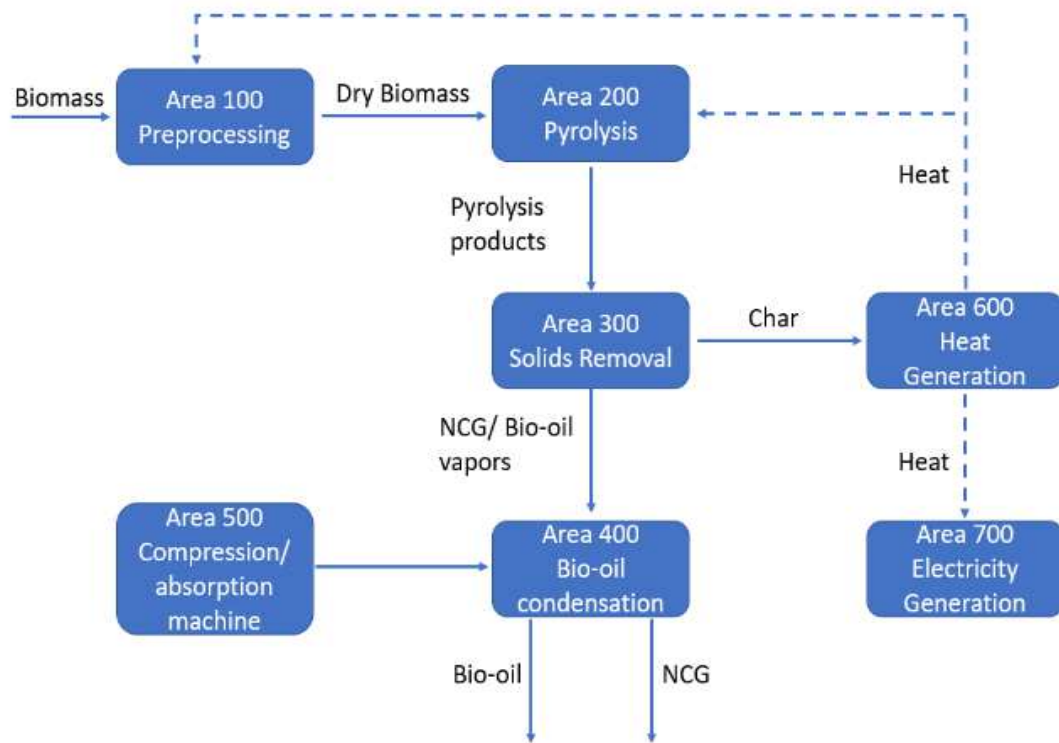
303

304

**Figure 5.** Methodology flow chart

305 Process overview can be seen in Figure 6. It is divided into seven major technical  
306 parts: (i) Preprocessing of feedstock (Area 100); (ii) Bio-oil production via catalytic fast  
307 pyrolysis (Area 200); (iii) Solids removal (Area 400); (iv) Bio-oil condensation (Area 400);  
308 (v) Compression/absorption machine (Area 500); (vi) Heat generation (Area 600); (vii)  
309 Electricity generation (Area 700).

310 In the feed processing section (Area 100), wet biomass is ground to less than 2 mm  
311 and then dried to reduce the moisture from 20% to 4% to meet the feed requirements of  
312 pyrolysis reactor. Pyrolysis takes place in Area 200 where OMWS is converted to bio-oil,  
313 biochar and non-condensable gases (NCG). The pyrolysis products are then fed into solids  
314 removal section (Area 300), which separates the solid particles (catalyst and biochar) from the  
315 hot bio-oil vapors and gases. The condensation of bio-oil vapors is achieved in the liquid  
316 recovery section (Area 400), using a compression refrigeration machine or an absorption  
317 refrigeration machine (Area 500). The biochar separated from bio-oil vapors is combusted in  
318 heat generation section (Area 600) to regenerate catalyst and produce heat (flue gases) to be  
319 used for drying of wet biomass and fast pyrolysis process.



320

321

**Figure 6.** Process overview

322 *2.3.1- Model Development*

323 The model is divided into different subsections (Area 100 - Area 700) for better  
 324 elaboration. Aspen Plus flowsheet can be seen in Figures 9 and 10. A heat exchangers  
 325 network is presented in Figure 11. HX-1 and HX-2 are the first and second condensers, HX-3  
 326 is for heating the fluidizing gas, HX-4 is employed for steam production and HX-5 is used to  
 327 heat the air for biomass drying.

328 *2.3.1.1- Feedstock preparation (Area 100)*

329 Olive mill wastewater sludge (OMWS) collected from Sfax, Tunisia with an initial size  
 330 of 200 mm is supplied to two hammer mills separated by a screen for particle separation. The  
 331 biomass is ground to 2 mm as required by pyrolysis reactor. The exiting wet biomass with  
 332 initial moisture content of 20% is dried in a convective dryer at an operating temperature of  
 333 120°C to reduce the moisture content to 4%. The heat for drying purpose is supplied by flue  
 334 gases coming from combustion of biochar (Area 600). The dried biomass is mixed with 20% of

335 biochar to make it less sticky and fed into the pyrolysis reactor smoothly. Table 1 summarizes  
336 properties of OMWS [35].

#### 337 *2.3.1.2- Pyrolysis (Area 200)*

338 In the pyrolysis section, pre-treated biomass is converted into bio-oil vapors, biochar,  
339 and non-condensable gases (NCG) in two virtual stages as discussed in section 3.2.1. The  
340 pyrolysis reaction was modelled using kinetic parameters derived from Agblevor et. al. [35]  
341 experimental findings. High-efficiency cyclones separate biochar from a mixture of gas and  
342 vapors, which is then fed into a combustor.

343 The heat required for the pyrolysis reaction is provided by char combustion in Area  
344 600. The residual heat is used to dry wet biomass and to produce superheated steam, which is  
345 then extended to generate 0.6 MW of electricity. The pyrolysis product mass flow rates are  
346 given in Table 12.

#### 347 *2.3.1.3- Solids Removal Area (Area 300)*

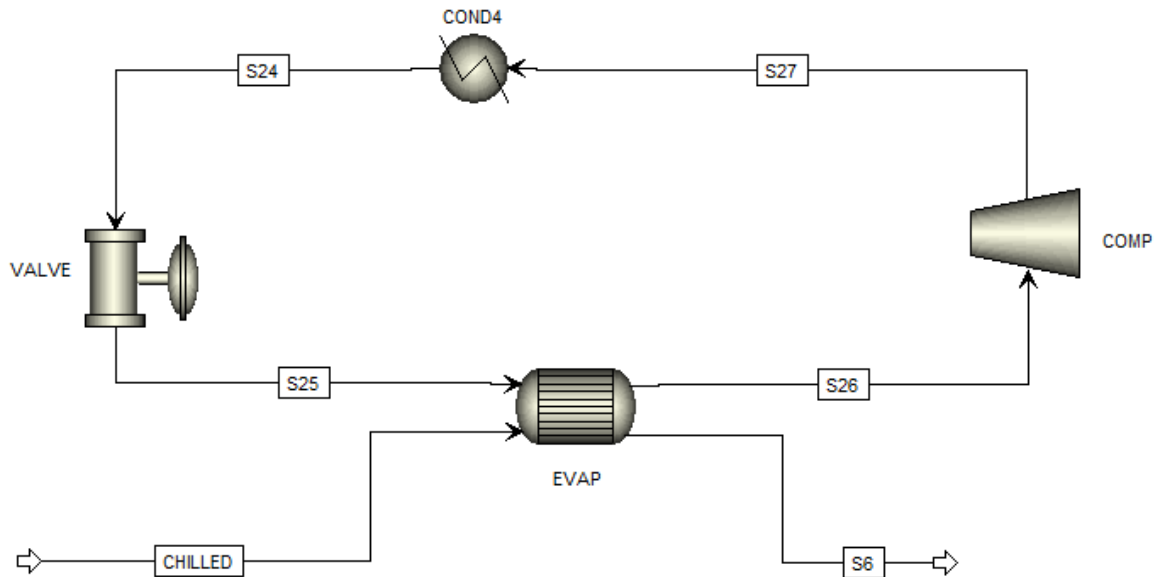
348 In Area 300, a high-performance cyclone separates the entrained catalyst fines and  
349 biochar from the gases and vapors, achieving a separation efficiency of 0.9. To completely  
350 remove the biochar and catalyst particulates from the products, another hot gas filter is  
351 employed.

#### 352 *2.3.1.4- Bio-oil condensation (Area 400)*

353 The hot product gases pass through the first condenser at 400°C and leave the first  
354 condenser at around 100°C condensing about 70% of bio-oil. About 685 kW of heat is removed  
355 in the first condenser. The cooled products are sent to another condenser where they are cooled  
356 to around 40°C and remaining bio-oil and water are condensed. In the second condenser, 237  
357 kW of heat is removed. The remaining fraction of bio-oil vapors is passed through an  
358 electrostatic precipitator to quench the bio-oil.

359 2.3.1.5- Refrigeration machine (Area 500)

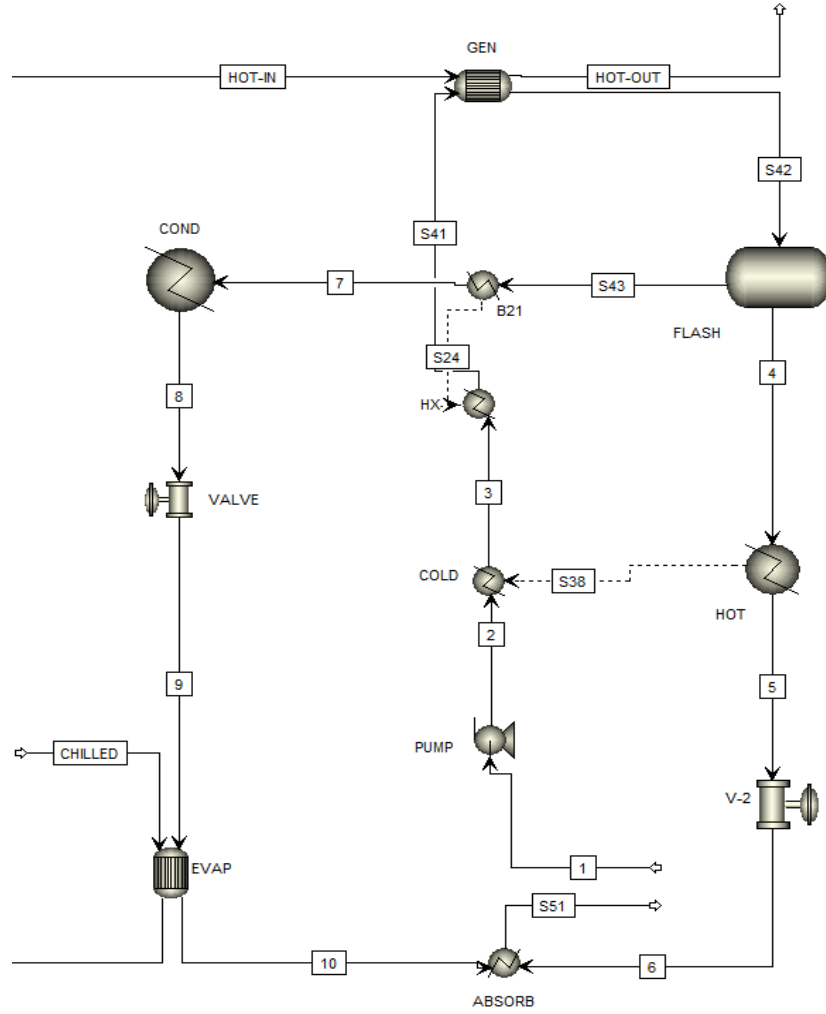
360 Two cooling machines were modelled in this study: (i) Vapor compression refrigeration  
361 machine (scheme-1) (ii) absorption refrigeration machine (LiBr-H<sub>2</sub>O) (scheme-2). In scheme-1,  
362 a conventional vapor compression refrigeration system is developed. The system is modelled  
363 with a compressor, condenser, valve and a heat exchanger (evaporator). Total cooling load  
364 required for both condensers is 922 kW. The refrigerant employed in the simulation for the  
365 refrigeration is R-22 and *REFPROP* is used as base method. Annually 5.4 million kWh of  
366 energy is removed in the first condenser and 1.8 million kWh in the second condenser.



367

368 **Figure 7.** Compression refrigeration machine

369 In scheme-2, the absorption refrigeration machine operates by recovering heat from the  
370 first condenser. The absorption machine is modelled for a cooling capacity of 237 kW. The  
371 cooling produced is used to cool down the pyrolysis products in the second condenser. The  
372 absorption system is modelled on the work of Somers et. al. [44]. Because the operating  
373 parameters and fluids being modeled with this approach are designed for electrolytes, the  
374 activity coefficient property method in ASPEN (*ELECNRTL*) is used for the water/LiBr  
375 solution. [45]. The *steamNBS* tables were utilized for the pure water states [46].



376

377

**Figure 8.** Absorption refrigeration machine

378 *2.3.1.6- Catalyst Regeneration (Area 600)*

379

The biochar is treated as a non-conventional component in this model, so the ultimate

380

analysis of the biochar needs to be determined as well. The ultimate analysis of biochar is

381

computed by the elemental balance in OMWS, gaseous components from OMWS pyrolysis and

382

biochar. A general formula to calculate the percentage of carbon in biochar is given by

$$C_{biochar}\% = \frac{C_{OMWS}\% - \left( \frac{f_{CO}}{28} + \frac{f_{CO_2}}{44} + \frac{f_{CH_4}}{16} + \frac{f_{C_2H_6}}{30} \times 2 + \frac{f_{C_3H_8}}{44} \times 3 + \frac{f_{C_4H_{10}}}{58} \times 4 + \frac{f_{Biooil}}{MW_{biooil}} \times N_{Biooil} \right)}{f_{Biochar}} \quad (11)$$

383

The percentages of other elements are calculated in the same manner.

384

The combustion of biochar is given by following reaction

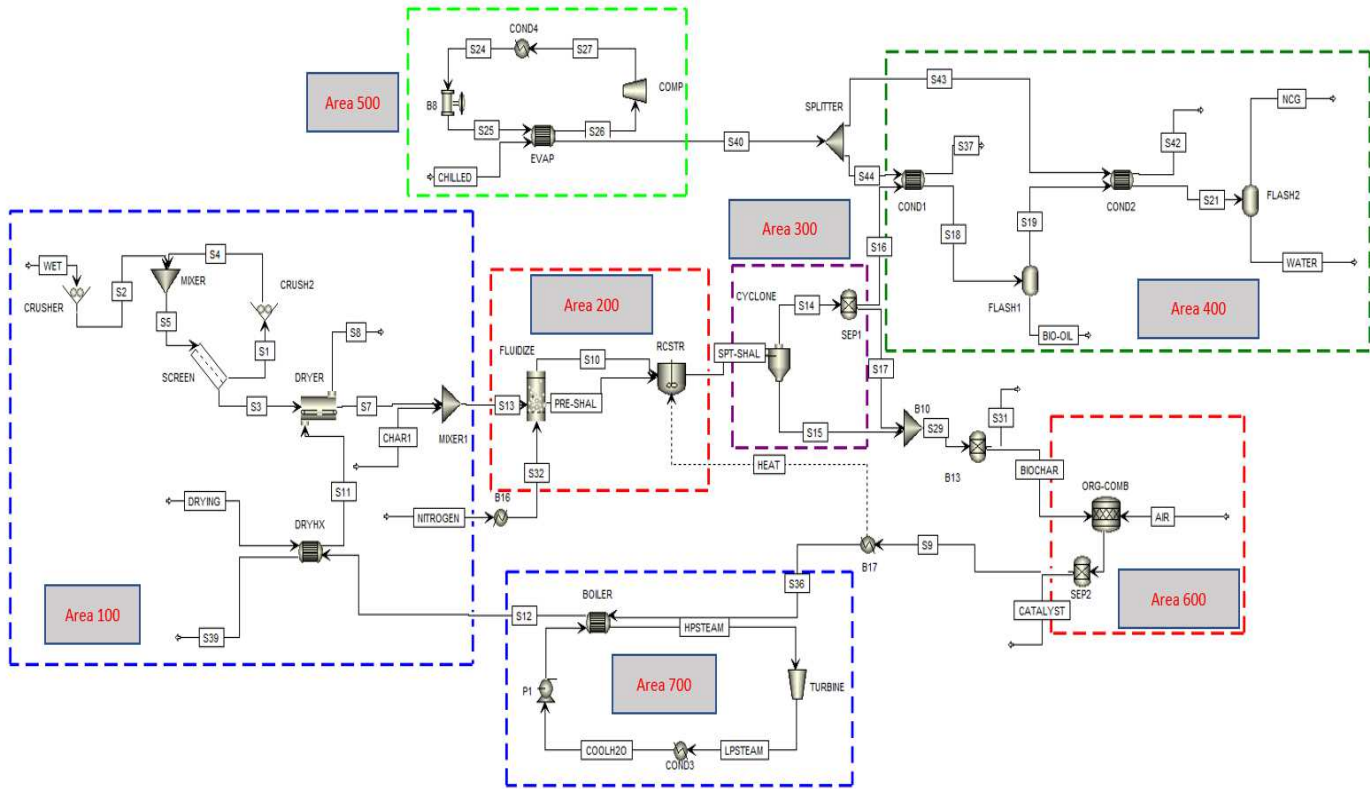


385 Biochar and catalyst exiting the cyclone are combusted in a combustor (*RStoic*). The  
386 biochar is combusted with excess air at a temperature of 1400°C. The heat generated is used to  
387 heat the pyrolysis reactor reducing the temperature of exhaust gases to 1000°C. In Area 700,  
388 these gases are utilized to produce superheated steam, which is then used to generate power.  
389 Finally, after steam generation, the exhaust gases are still hot to be used in drying the wet  
390 biomass in Area 100.

#### 391 2.3.1.7- *Electricity generation (Area 700)*

392 The heat generated by combustion of biochar in Area 600 is used to produce steam,  
393 which is then used to generate electricity. The steam power cycle was modelled using a steam  
394 turbine, a heat exchanger, a condenser, and a feed water pump. The *NBS/NRC* steam table in  
395 Aspen Plus was employed to model the thermodynamic properties of the water portion of the  
396 heat exchanger. Superheated steam was produced at 503°C and fed into the steam turbine to  
397 generate electricity. The steam turbine was specified at 95% mechanical efficiency and 80%  
398 isentropic [32].



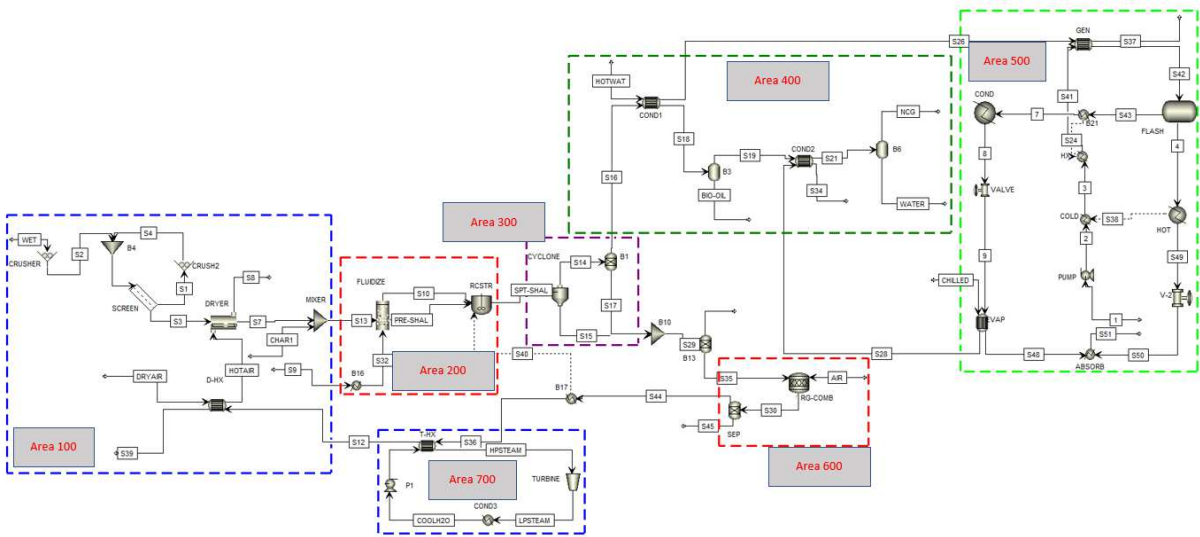


399

400

**Figure 9.** Process flow diagram with compression refrigeration machine

401



402

403

**Figure 10.** Process flow diagram with absorption refrigeration machine

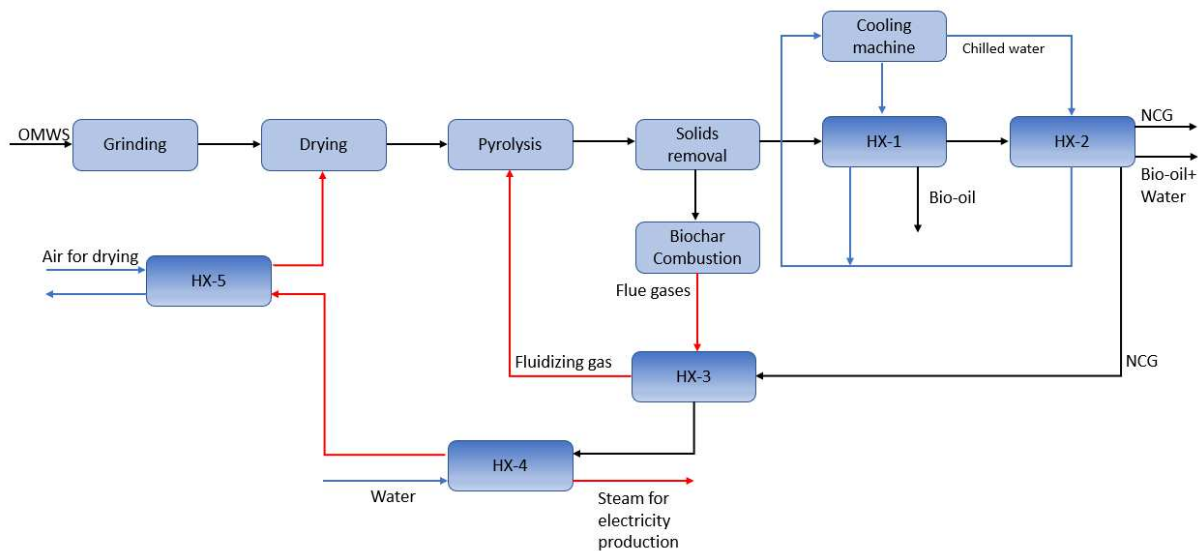


Figure 11. Heat exchangers network

#### 2.4- Performance parameters

Energy efficiency of the system is calculated by dividing energy output from the system by the energy input to the system. The energy efficiency formula is shown in eq. 13 [32].

$$\eta_{plant} = \frac{\dot{m}_o \cdot LHV_o + W_o}{\sum_i (\dot{m}_i \cdot LHV_i) + \sum W_i + Q_i} \quad (13)$$

where  $\dot{m}_o$  represents the mass flow rate of bio-oil and gaseous products and  $LHV_o$  represents the corresponding lower heating value.  $W_o$  represents the electricity generated by the turbine. Similarly,  $\dot{m}_i$  and  $LHV_i$  are the biomass flow rate and lower heating value respectively.  $W_i$  is total power required to operate the complete system including pumps, dryer, grinder, compressor and cyclones. Th hot utility utilized in the plant is represented by  $Q_i$ .

Absolute average deviation  $e$  between simulated and experimental results is given by [47]:

$$e (\%) = 100 \times \left( \sum_i^N \frac{|Y_{i,sim} - Y_{i,exp}|}{Y_{i,exp}} \right) / N \quad (14)$$

where  $Y_{i,sim}$  is the quantity of a product calculated by simulation model and  $Y_{i,exp}$  is the experimental quantity of a product.

417 2.4.1- Process Economics

418 2.4.1.1- Cost Estimation

419 Aspen Process Economic Analyzer (APEA) was used to size equipment and estimate  
420 costs. To conduct sizing measurements and approximate equipment procurement costs, the unit  
421 operations modelled in Aspen Plus are sent to APEA where they are mapped and sized to the  
422 desired equipment cost models. The costs of pyrolysis reactor and regenerator were calculated  
423 using scaling equation as stated by Wright et al. [33].

$$C_1 = C_o \cdot \left(\frac{S_1}{S_o}\right)^{0.6} \quad (15)$$

424 where  $C_1$  is the new calculated cost with the size of  $S_1$  and  $C_o$  is the base cost with the size of  
425  $S_o$ . The equipment cost is updated to current year (2021) by using the Chemical Engineering  
426 Plant Cost Index (CEPCI) by employing the following equation [9].

$$\text{New equipment cost} = \text{Base equipment cost} \times \frac{\text{2021 cost index value}}{\text{Base year cost index value}} \quad (16)$$

427 CEPCI for 2021 is listed as 754.7 and for 2018 is 603.1 [48].

428 Table 6 shows the assumptions made during the calculation of total operating cost.

429 **Table 6.** Operating cost parameters

Material	Cost
Biomass cost [€/t]	30
Catalyst [€/kg]	3
<b>Utilities</b>	
Electricity [€/kWh] [49]	0.065
Cooling water [€/m <sup>3</sup> ]	0.032

430

431 The project will be based in Tunisia, and new tax legislation has been enacted as a result of  
432 the devastating economic impact of Covid-19 on the nation. According to the 2021 Finance

433 Law, a corporate income tax rate of 10% applies to investments in agriculture, fisheries,  
 434 handicrafts, pollution control, and so on, while a rate of 35% applies to the financial sector,  
 435 oil and gas, telecommunications etc. [50].

436 **Table 7.** Inputs for DCF analysis

<b>Economic Inputs</b>	
Required rate of return	10%
Plant life	20 years
Capital cost escalation	5%
Revenue escalation	5%
Operating cost escalation	3%
Income Tax	40%

437

438 **Table 8.** Variation in different parameters

<b>Parameter</b>	<b>Range</b>
Fuel yield [kg/year]	± 30%
Capital cost [€]	± 30%
Operating cost [€]	± 30%
Income tax [%]	10% to 60%
Discount rate [%]	0% to 40%

439

440 Total project investment was calculated using Peters and Timmerhaus's method [51] as  
 441 shown in Table 9. The capital cost of the pyrolysis plant is made up of direct and indirect costs,  
 442 as well as a contingency and location factor. Regional labor, supervisor, and service costs are  
 443 included in the cost model. Total installed cost (TIC) is approximated by 3.02 times the  
 444 purchased cost of equipment. Installation cost includes electrical wiring, plumbing, structures,

445 and other related costs. Indirect costs include contractor's fees, supervision and technical cost,  
 446 legal fees and construction costs. It is calculated at a rate of 0.89 times the total purchased  
 447 equipment cost.

448 **Table 9.** Total project investment estimation method [20,51]

Parameter	Value
Total purchase equipment cost (TPEC)	100% TPEC
Total installed cost (TIC)	302% TPEC
Indirect cost (IC)	89% TPEC
Total direct and indirect cost (TDIC)	TIC + IC
Contingency	20% TDIC
Fixed capital investment (FCI)	TDIC + contingency
Location factor (LF)	10% FCI
Total project investment (TPI)	FCI + LF

449

450 *2.4.1.2- Profitability analysis*

451 The discounted cash flow approach was used to assess the profitability of all process  
 452 schemes. The minimum fuel selling price (MFSP) is calculated by setting the NPV to zero in  
 453 equation 17.

$$NPV = -C_T + \sum_{n=1}^{N=t} \frac{\phi \dot{m}(1 - T_n) - O_n}{(1 + r)^n} \quad (17)$$

454 where  $C_T$  represents the initial capital investment,  $\phi$  is the fuel price, annual fuel yield of  
 455 plant is specified by  $\dot{m}$ , annual operating cost is represented by  $O_n$ ,  $T_n$  is annual income tax  
 456 and  $r$  is the required rate of return. The plant is assumed to be operational for a 20-year period  
 457 (t) in the DCF analysis.

#### 458 2.4.1.3- Sensitivity Analysis

459 Sensitivity analysis is a method for assessing the profitability effect of improvements  
460 in procedure and economic parameters. The effect of key parameters on the MFSP, such as  
461 bio-oil yield, capital investment, operational cost, discounted rate and income tax was  
462 investigated. These parameters were selected because they have a clear connection to  
463 profitability; in other words, the MFSP of bio-oil is closely related to these parameters. A  
464 30% spectrum is used in the sensitivity analysis. Although the specified spectrum of the  
465 sensitivity analysis allows for individual evaluation of uncertainty in parameter estimates, it  
466 does so in a deterministic fashion that ignores the studied parameters.

### 467 **3- Results and discussions**

#### 468 3.1- Model Validation

469 Simulations were performed in Aspen Plus based on fluidized bed data for non-  
470 catalytic and catalytic fast pyrolysis processes. To determine the accuracy of the developed  
471 fluidized bed fast pyrolysis model, bio-oil, bio-char, and NCG yields were compared with the  
472 experimental results reported by the work of Agblevor et al. [35]. The fast pyrolysis process  
473 with and without catalyst was simulated under identical conditions in experimental studies of  
474 Agblevor et. al. [35] by using input and output variables such as reactor temperature,  
475 characteristics of biomass, catalyst, and the flow rate of feedstock, etc.

##### 476 3.1.1- Non-Catalytic fast pyrolysis

477 After defining the proximate, ultimate and chemical analyses of each component used  
478 in the proposed model, the simulation was performed at different pyrolysis temperatures 400,  
479 450 and 500°C using Aspen Plus to compute the yields of the different products; bio-oil,  
480 biochar, NCG and water. The obtained results of the product yields are presented in Figures  
481 12, 13 and 14 compared with experimental data. The absolute average deviation (AAD) at

482 different temperatures is illustrated in Table 10. It depicts the closeness of simulation results  
 483 to the experimental data.

484 As shown in Figures 12, 13 and 14, the trend of product yields between simulation  
 485 results, for non-catalytic fast pyrolysis, satisfactorily represents the experimental data with  
 486 AAD for bio-oil, biochar, NCG, and water range from 0.53% to 1.95%, 1.52% to 2.91%,  
 487 1.96% to 2.70% and 3.39% to 9.77% respectively. In addition, the sensitivity of the product  
 488 yields on pyrolysis temperature was simulated and investigated. The simulation results  
 489 depicted in Figures 12-14 show that the yield of bio-oil increases with increasing reaction  
 490 temperature and reaches a maximum of 36.6 wt.% at a pyrolysis temperature of 450°C. The  
 491 low bio-oil yield obtained from the fast pyrolysis of OMWS is expected since the composition  
 492 of the polymers which constitute OMWS is not the same and the properties of OMWS have  
 493 high ash content which favors charring reaction [52]. Above 450°C, the bio-oil yield  
 494 decreases slightly with increasing temperature. Therefore, the optimum pyrolysis temperature  
 495 for bio-oil production from OMWS is 450°C which is low if compared with other  
 496 lignocellulosic biomasses cited in the literature. This difference is due to the chemical  
 497 composition of biomass which affects not only the pyrolysis product yield but also pyrolysis  
 498 temperature.

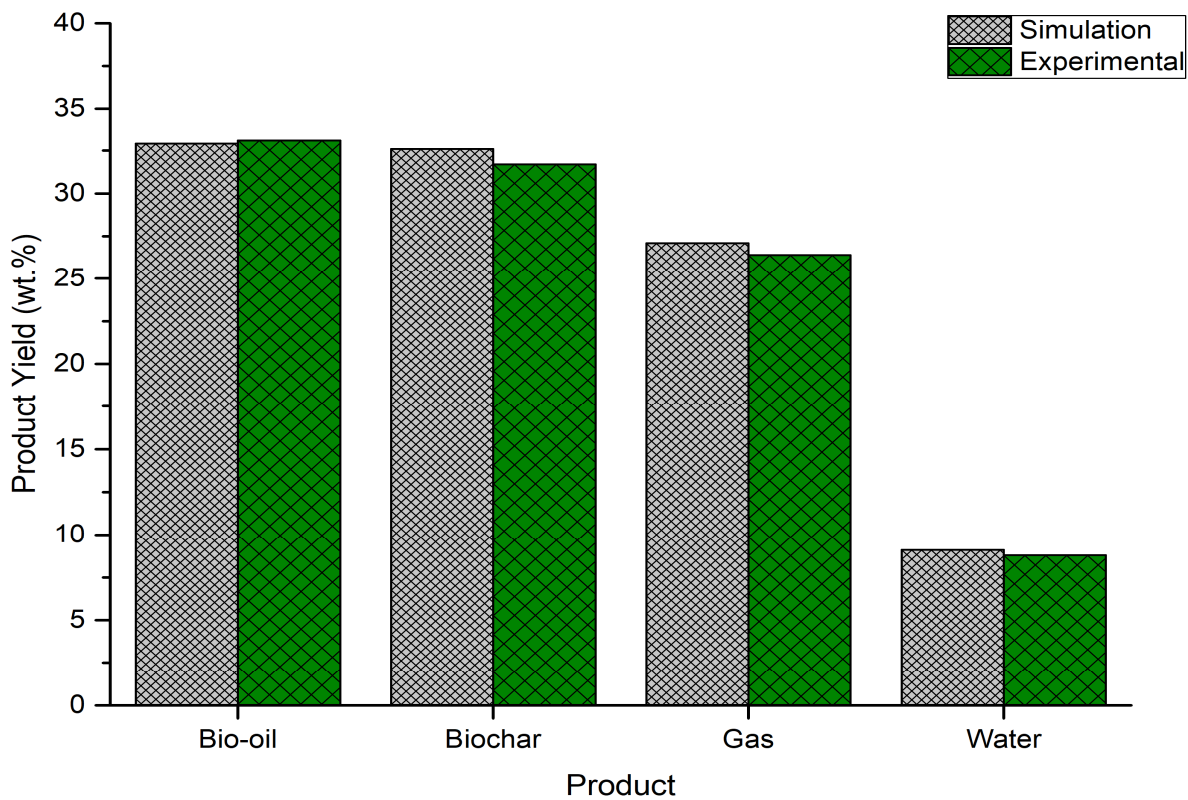
499 **Table 10.** Absolute average deviation (*e*) for different temperatures

Product	<i>e</i> (%)	<i>e</i> (%)	<i>e</i> (%)
	400°C	450°C	500°C
Bio-oil	0.53	1.95	0.99
Biochar	2.91	1.52	1.84
NCG	2.70	2.40	1.96
Water	3.46	3.39	9.77
Overall	2.40	2.32	3.64
Global		2.78%	

500

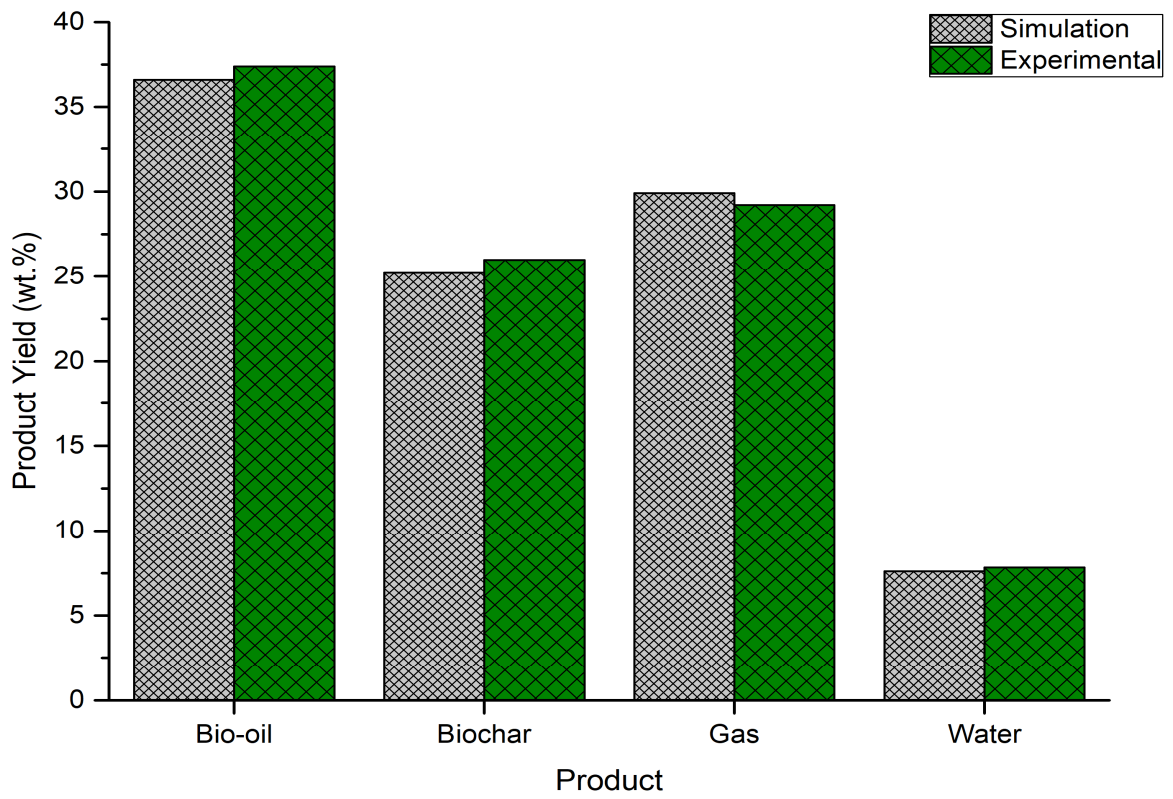
501 Furthermore, the product yields analysis of non-catalytic pyrolysis shows the decrease  
502 of biochar and the increase of the gas yield when the pyrolysis temperature increases. This  
503 can be explained by the secondary reactions of decomposition of the solid formed during the  
504 fast pyrolysis to produce bio-oil and gas. It can be also noted that the increase in the gas yield  
505 and decrease in the bio-oil yield above 450°C is due to the secondary cracking reaction  
506 occurring in the vapors.

507 In general, the water is yielded from the pyrolysis process at a temperature below  
508 200°C and is present among the products of OMWS since the water gas shift reaction does  
509 not take place in the range temperature between 400 to 500°C. In addition, it can be observed  
510 that the yield of pyrolytic water is slightly affected by the pyrolysis temperature.



511  
512 **Figure 12.** Comparison between simulation and experimental yields at 400°C  
513



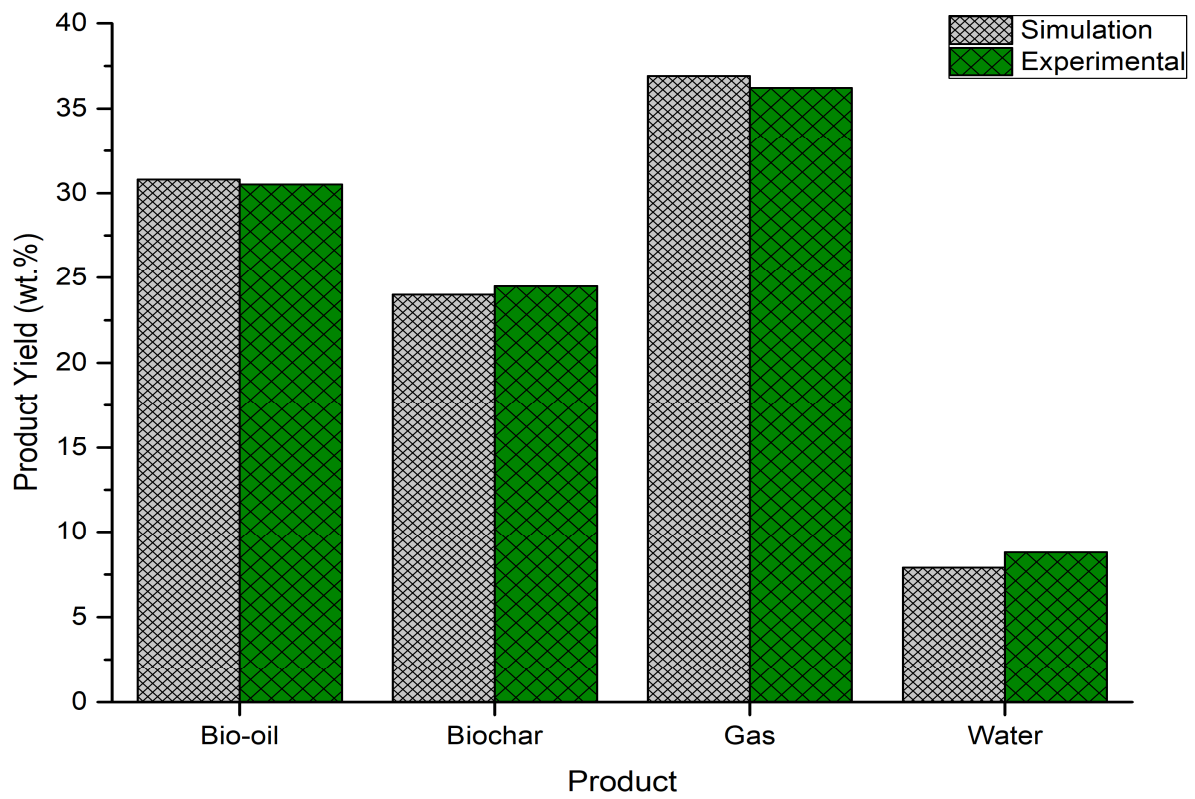


514

515

**Figure 13.** Comparison between simulation and experimental yields at 450°C

516



517

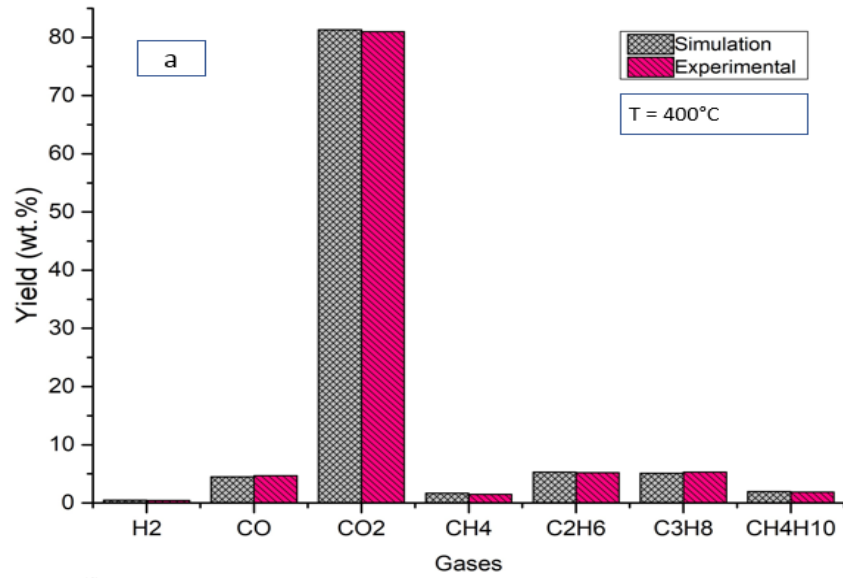
518

**Figure 14.** Comparison between simulation and experimental yields at 500°C

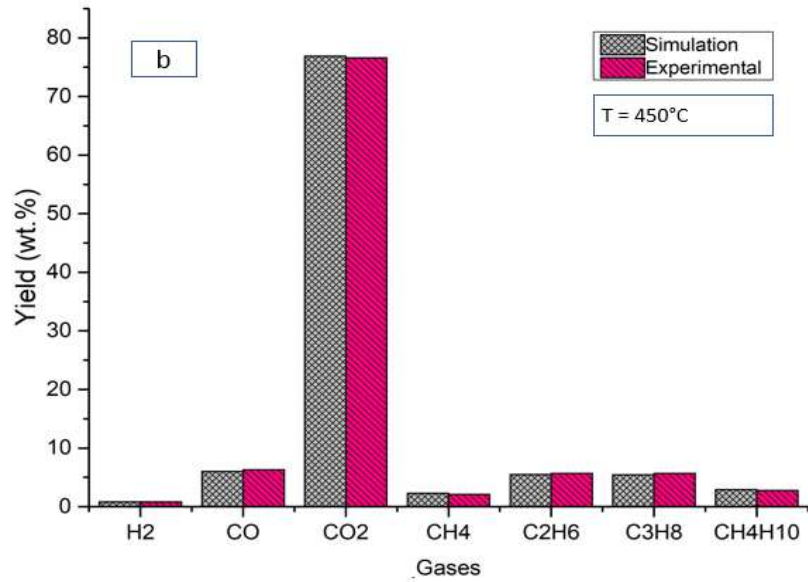
519 The effect of pyrolysis temperature on the gas composition was also simulated and  
520 was depicted in the Figure 15 with the experimental results. Model simulations in the range of  
521 pyrolysis temperature between 400 to 500°C show that the product gases distribution of the  
522 non-catalytic fast pyrolysis of OMWS contains the notable gas species: carbon dioxide (CO<sub>2</sub>),  
523 carbon monoxide (CO), ethane (C<sub>2</sub>H<sub>6</sub>), propane (C<sub>3</sub>H<sub>8</sub>), butane (C<sub>4</sub>H<sub>10</sub>) and methane (CH<sub>4</sub>)  
524 but hydrogen (H<sub>2</sub>) is found in trace amounts. The deviations of the model predictions from the  
525 experiments are less noticeable for all gas species at different pyrolysis temperatures.  
526 Figure 15a shows that CO<sub>2</sub> represents 81.09 wt.% of total gases at temperature 400 °C thanks  
527 to the fatty acids compounds present in the OMWS and the gases CO and CH<sub>4</sub> represent  
528 4.71% and 1.50% respectively because their production is carried out at higher temperature.  
529 The presence of CH<sub>4</sub> within the composition of gases is useful and interesting as a source of  
530 fuel.

531 As shown in Fig. 15a-c, CO<sub>2</sub> yield decreased and the yield of CO, CH<sub>4</sub>, C<sub>2</sub>H<sub>6</sub>, C<sub>3</sub>H<sub>8</sub>  
532 and C<sub>4</sub>H<sub>10</sub> slightly increased when the temperature increased. The diminution of the CO<sub>2</sub> is  
533 due to its decomposition to generate more CO. This result is reported Pavier et. al. [53] who  
534 studied the effect of temperature parameter on the thermochemical treatment of biomass. No  
535 significant effect is observed by the increase of the temperature on H<sub>2</sub> gas.

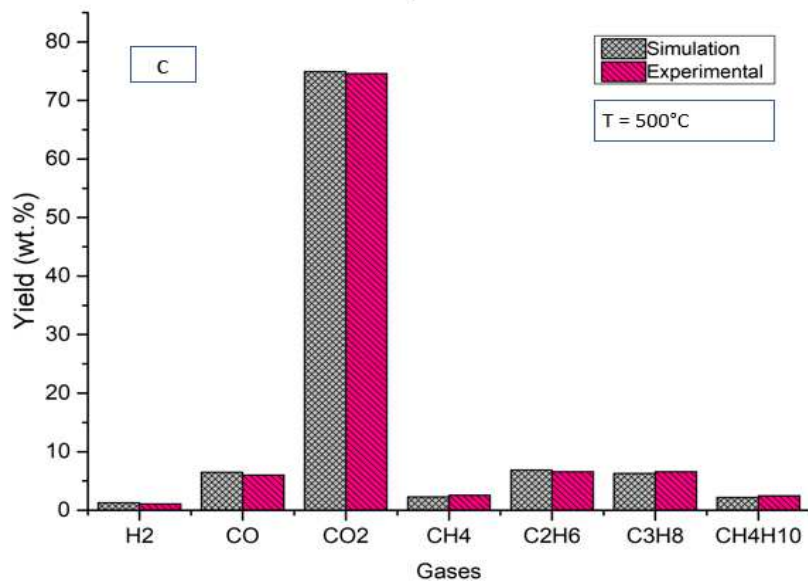
536



537



538

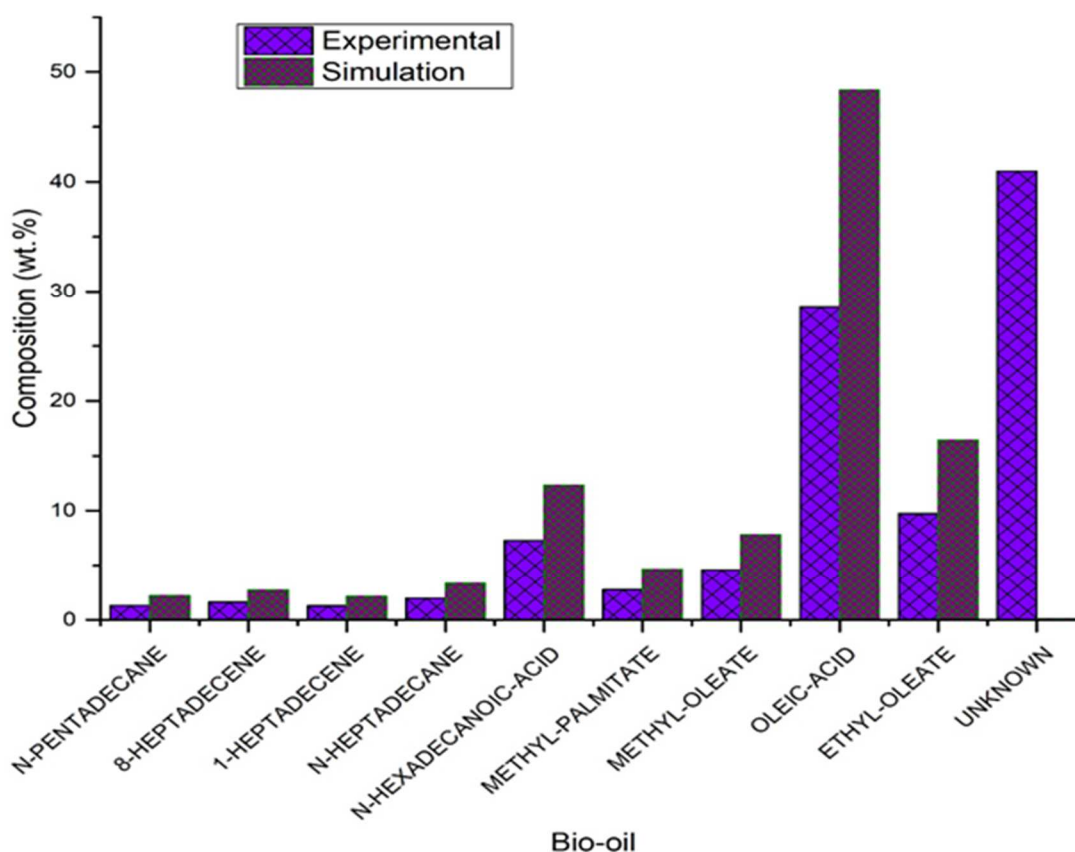


539

540

**Figure 15.** Distribution of gas composition during non-catalytic fast pyrolysis.

541 In order to demonstrate how the Aspen model performs in predicting individual bio-oil  
542 compounds for non-catalytic fast pyrolysis, model predictions at 450°C were compared with  
543 experimental data as shown in Figure 16. It can be seen that the simulation results have  
544 similar experimental results for the bio-oil composition. In addition, by comparing the  
545 experimental data and simulation results for the yield of each compound of the bio-oil, it can  
546 be noted that the higher composition of each individual compound in the simulation model is  
547 due to the fact that it was not possible to determine the identity of some compounds  
548 experimentally. Subsequently, the model takes into account these compounds as unknown  
549 compounds and to accommodate these unknown compounds, the weight percentage of known  
550 compounds was higher in the simulation model.  
551



552

553 **Figure 16.** Bio-oil composition at 450 °C for non-catalytic fast pyrolysis.

554

555

556 3.1.2- Catalytic fast pyrolysis

557 The non-catalytic fast pyrolysis results of OMWS investigated by Agblevor et. al. [35]  
558 showed that the pyrolytic OMWS bio-oil had high oxygen content and viscosity. To upgrade  
559 the quality of this bio-oil, Agblevor et. al. [35] investigated in situ catalytic fast pyrolysis  
560 process using red med as a catalyst. In this case, the Aspen Plus model was also developed to  
561 simulate the catalytic fast pyrolysis of OMWS at the same temperature used in non-catalytic  
562 pyrolysis. The model was validated against the experiments of Agblevor et. al. [35] conducted  
563 in a fluidized bed pyrolyzer. The simulation results with experimental data of the products  
564 yield distribution are shown in Figures 17, 18, and 19 and the absolute average deviation  
565 values are depicted in Table 11. It can be seen that the simulation model of the biochar and  
566 water yield distribution correlates better with experimental data of Agblevor et. al. [35]  
567 particularly at temperatures 450 and 500°C (AAD < 3%). At temperature 400 °C, water yield  
568 in the simulation is 12.3% while in the experiment is 11.3% resulting the AAD about 8.85%.  
569 Correlation between the model and experimental data reported by Agblevor et. al. [35] was  
570 found to be satisfactory for bio-oil and gas yield results at different pyrolysis temperatures in  
571 the range of 400 – 500°C showing that the AAD is lower than 4.2%. However, the overall  
572 AAD values of products yields at temperatures 400, 450 and 500 °C are 4.78%, 3.27% and  
573 2.56%, respectively and the global AAD value comes out to be 3.54%.

574 Based on the previously described statistical analysis, it was discovered that the model  
575 was valid for three temperatures and could be confidently utilized for economic analysis at  
576 these temperatures.

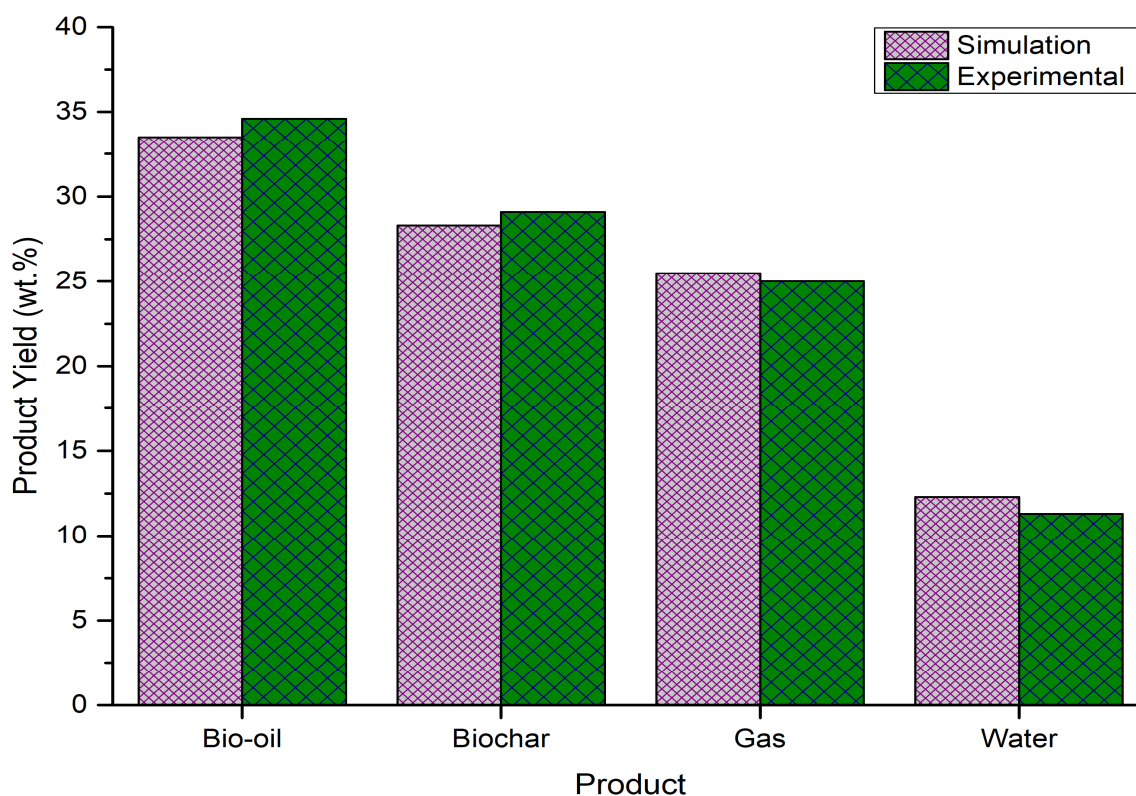
577 **Table 11.** Absolute average deviation (e) for different temperatures

Product	<i>e</i> (%)	<i>e</i> (%)	<i>e</i> (%)
	400°C	450°C	500°C
Bio-oil	3.28	4.17	2.79
Biochar	5.02	2.66	2.64
Gas	1.87	3.64	3.70

Water	8.96	2.64	0.14
Overall	4.78	3.27	2.56
Global		3.54%	

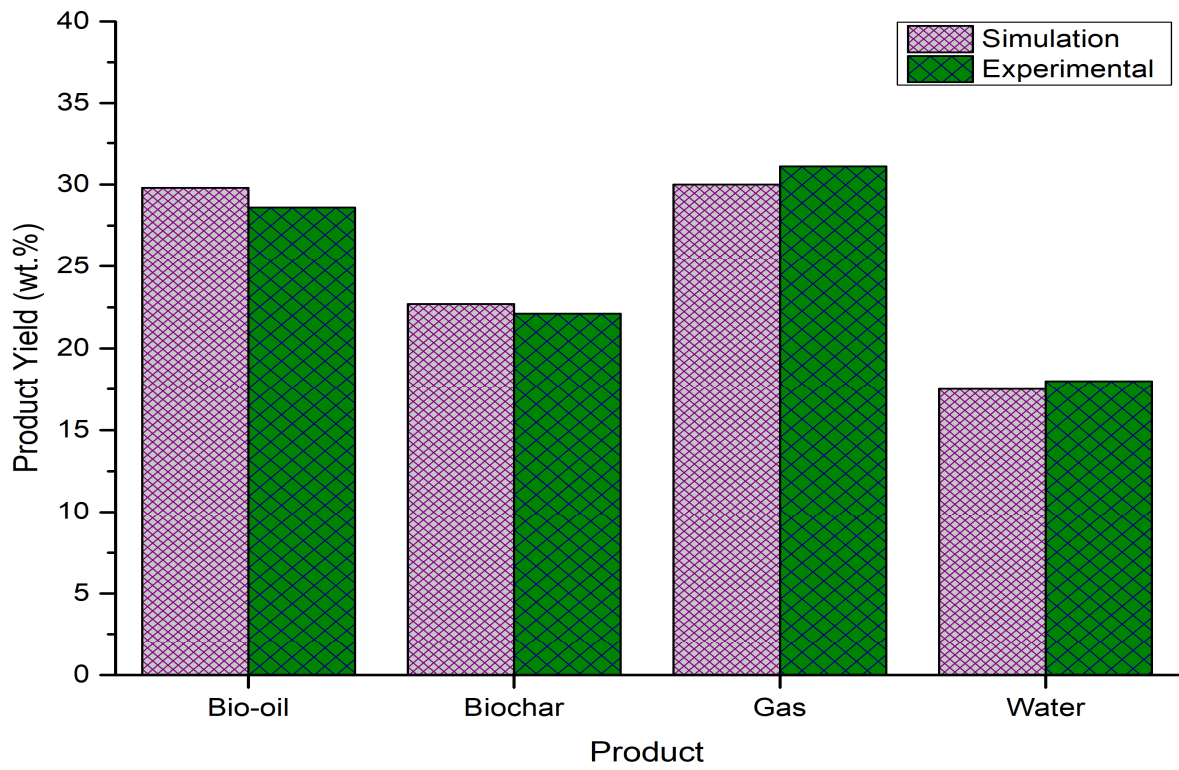
578

579 As shown in Figs. 17-19, bio-oil yield decreases when the temperature increases from  
580 400 to 450 °C and remains practically constant up to 500 °C while the gas yield increases  
581 with the temperature and the biochar yield decreases. The water content in the liquid product  
582 increases with the temperature up to 450 °C and decreases up to 500 °C. This result can be  
583 explained by the triggering of the secondary vapor cracking reactions such as  
584 decarboxylation, decarbonylation, ketonization and cracking of bio-oil to produce pyrolysis  
585 water and gas under red mud catalyst effect. In addition, the decrease in the pyrolysis water  
586 content at 500°C may be explained by the effect of the catalyst which starts the water gas shift  
587 reaction. Compared with the simulation results for non-catalytic pyrolysis in the range of 450-  
588 500 °C, the decrease of the biochar yield is due to thermal decomposition effect.



589

590 **Figure 17.** Comparison between simulation and experimental yields at 400°C

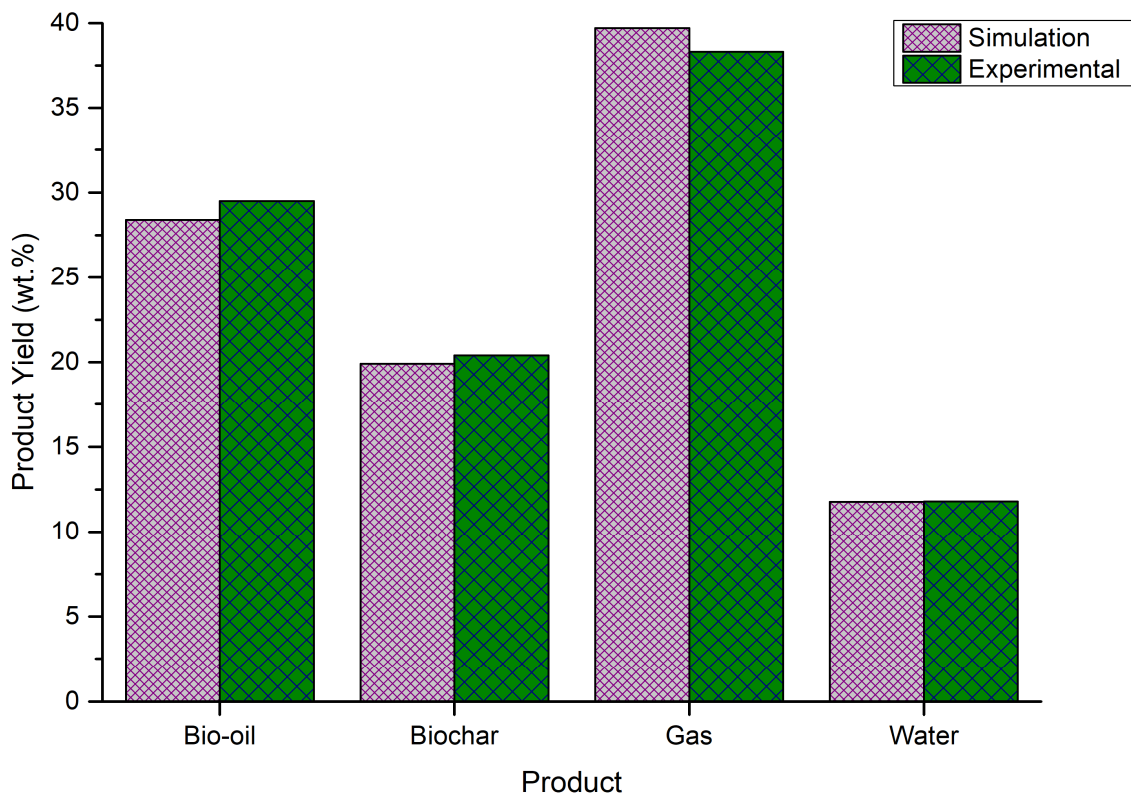


591

592

**Figure 18.** Comparison between simulation and experimental yields at 450°C

593



594

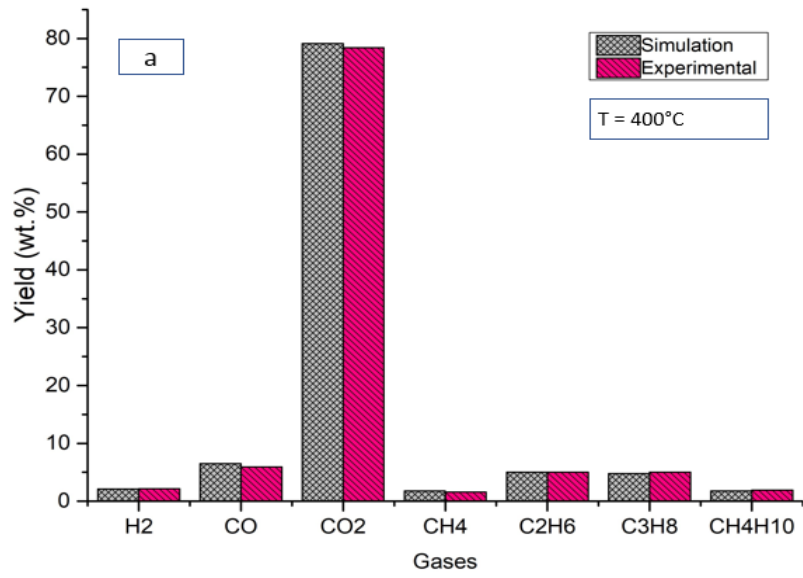
595

**Figure 19.** Comparison between simulation and experimental yields at 500°C

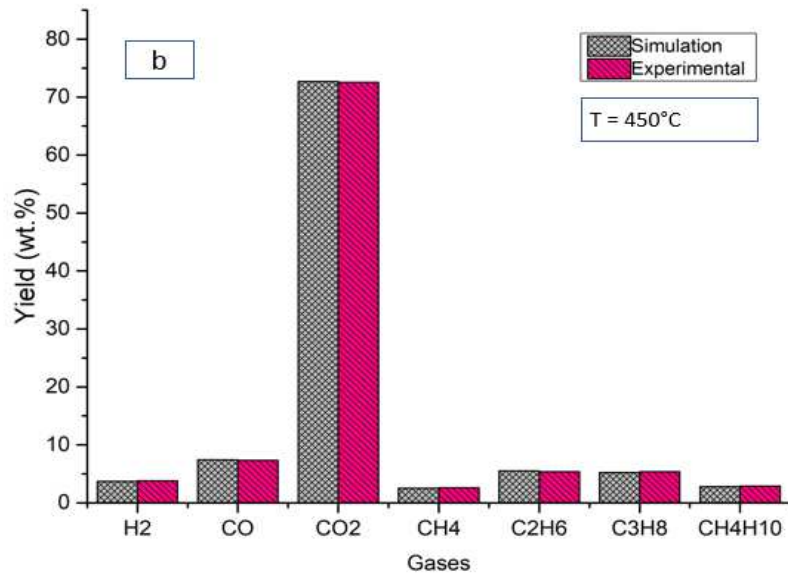
596

597           The composition of fast catalytic pyrolysis product gases predicted from Aspen plus-  
598 based simulation was also investigated and compared with the experimental data. The  
599 distribution of the gas composition with different pyrolysis temperatures is shown in Figure  
600 20. It can be observed that the model predictions were found to correlate well with  
601 experimental data for each gas species at different pyrolysis temperatures. Similar gas species  
602 are reported by non-catalytic fast pyrolysis simulations but have different yields under the red  
603 mud catalyst effect. As shown in Figure 20a-c, the yield of CO<sub>2</sub> decreased from 78% at 400°C  
604 to 66.1% at 500°C whereas the CO, H<sub>2</sub>, and CH<sub>4</sub> increased from 6.45%, 2.1%, and 1.6% at  
605 400 °C to 11.8% 3.9% and 3.8% at 500 °C, respectively.

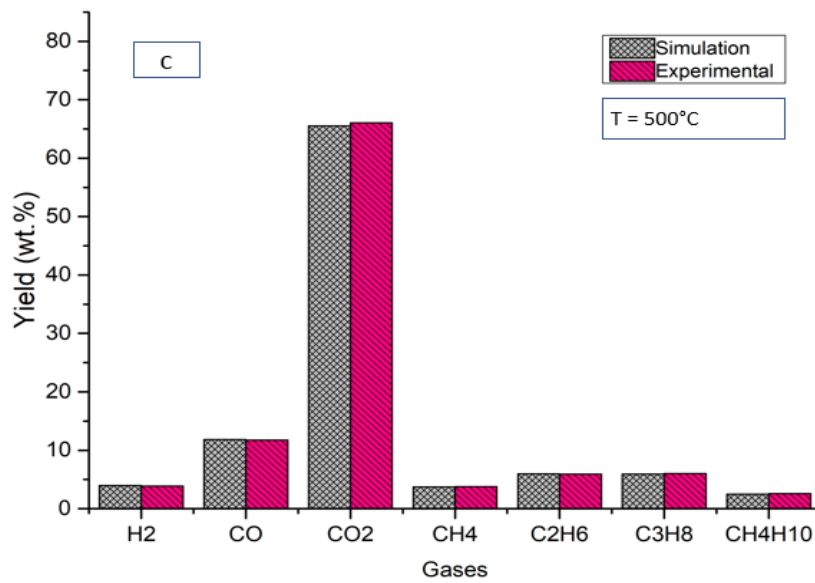




606



607



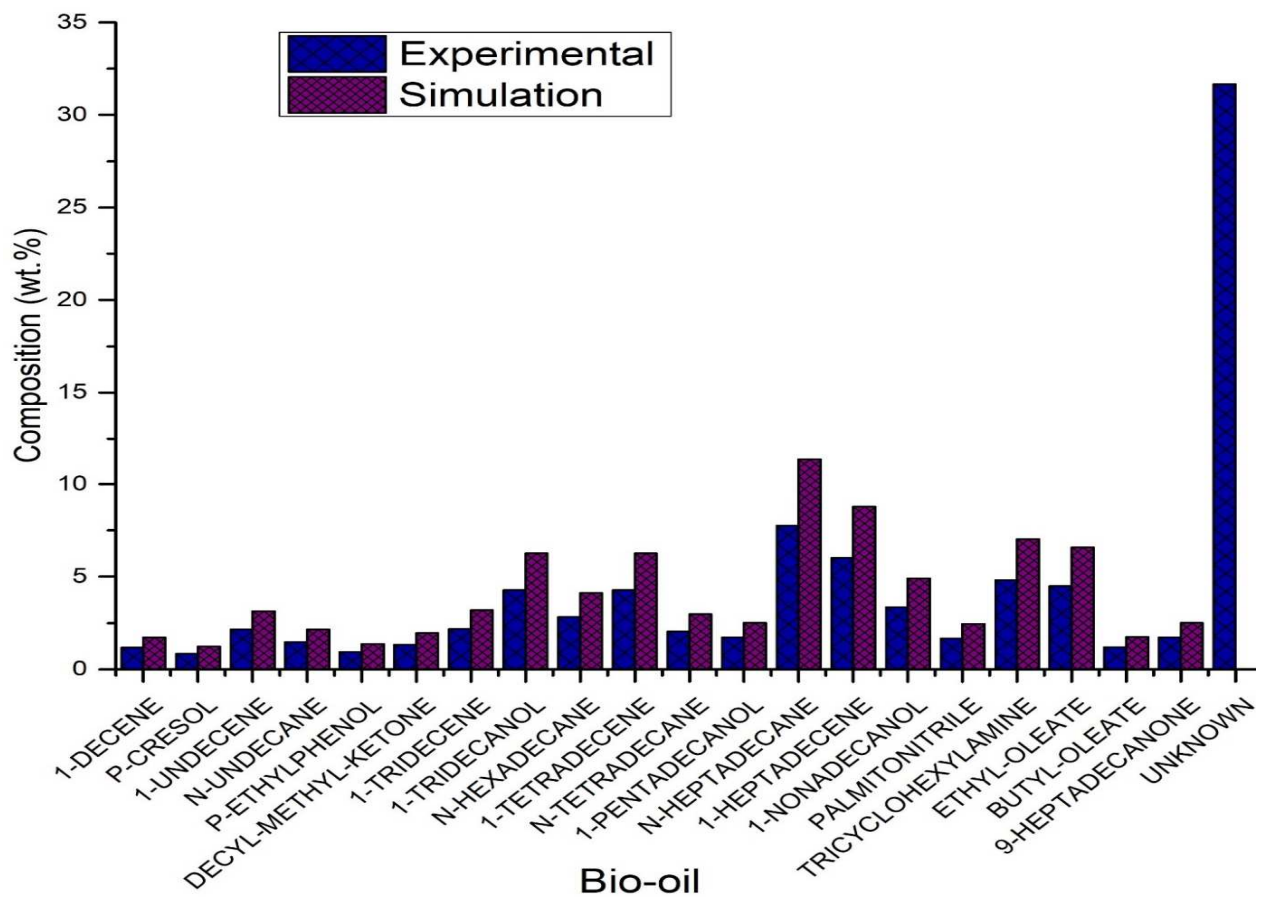
608

609

**Figure 20.** Gas composition of OMWS for catalytic pyrolysis

610 Figure 21 shows the composition distribution of catalytic bio-oil obtained at 450 °C. It  
 611 can be seen that the deviations between the model predictions and the experimental data are  
 612 noticeable for all bio-oil compositions. These deviations are due to the fact that apart from a  
 613 large number of compounds determined, there is still about 30% of bio-oil composition that  
 614 could not be determined experimentally. In addition, there are some compounds that could not  
 615 be found in the Aspen Plus directory so they were termed as unknown compounds. So, this  
 616 validation is attributed to the limitation of the model to simulate the compounds yields which  
 617 are present in the catalytic bio-oil.

618



619

620 **Figure 21.** Composition of bio-oil for catalytic fast pyrolysis at 450 °C.

621 *3.2- Techno-economic Assessment*

622 *3.2.1- Process performance*

623 The model processed 4,166 kg/h of wet OMWS and produced bio-oil at a rate of 1,366  
624 kg/h. Biochar was combusted to supply heat for the pyrolysis reactions and electricity  
625 production in an integrated steam cycle. As a result, the bio-oil production portion (Area 200) is  
626 self-sufficient in terms of energy and does not require additional utility heating [16]. In addition,  
627 Area 700 produced 603 kW of power. Since the reactor temperature for both process schemes  
628 was set to 400°C, there is no difference in fuel yields between the two process schemes.  
629 According to experimental results published by Agblevor et. al. [35], the same reactor yields  
630 were presumed for both schemes. Nonetheless, the two models vary in terms of electric power  
631 usage and capital costs. The discrepancy in energy efficiencies can be explained by the fact that  
632 the two systems used different amounts of electricity. In Section 3.2, the economic  
633 ramifications of the marginal difference in measured energy efficiencies are assessed. The  
634 mass and energy balances derived from the Aspen Plus simulation of the process are shown in  
635 Table 12.

636 **Table 12.** Mass and energy per hour basis

---

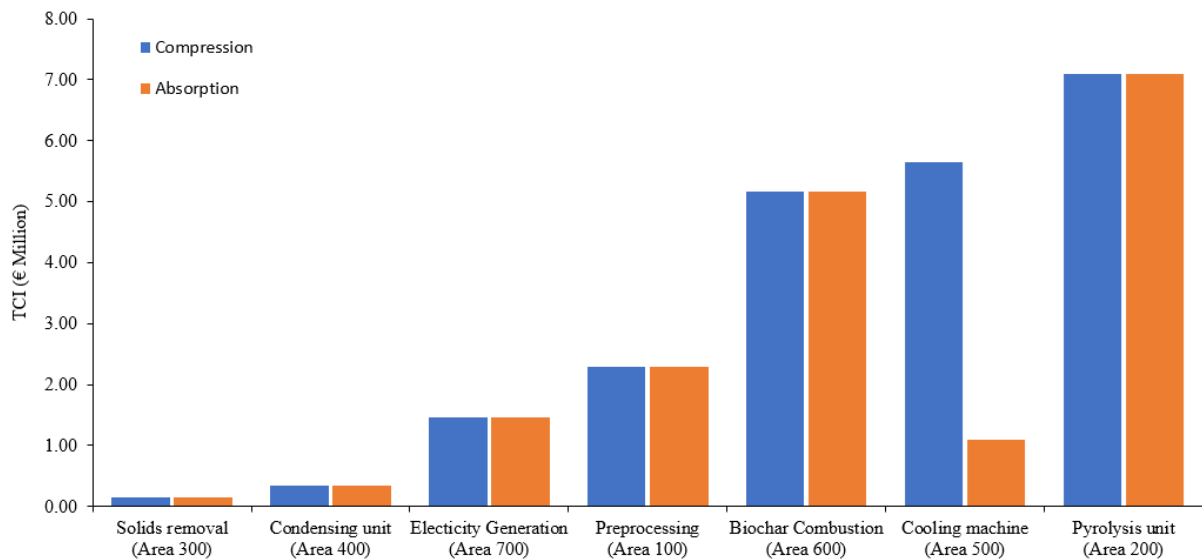
<b>Process inputs</b>	
Biomass (kg/h)	4,166
Electricity (kWh)	391
<b>Process outputs</b>	
Bio-oil (kg/h)	1,383
Biochar (kg/h)	1,168
NCG (kg/h)	1,012
Water vapors	343
Electricity (kWh)	603

---

637 3.2.2- Economic analysis

638 Figure 22 shows the comparison between proportions of total capital investment for the  
639 industrial scale pyrolysis plant for both schemes. The pyrolysis unit accounted for the  
640 maximum cost (about €7.10 million) while solids separation section constitutes the minimum  
641 capital cost (about €0.15 million). Overall, the total capital cost of the process is estimated to  
642 be €22.1 million for scheme-1 and €17.5 million for scheme-2. The higher capital cost  
643 observed in scheme-1 compared to scheme-2 is attributable to cost of vapor compression  
644 refrigeration machine which is significantly bigger than absorption refrigeration machine.

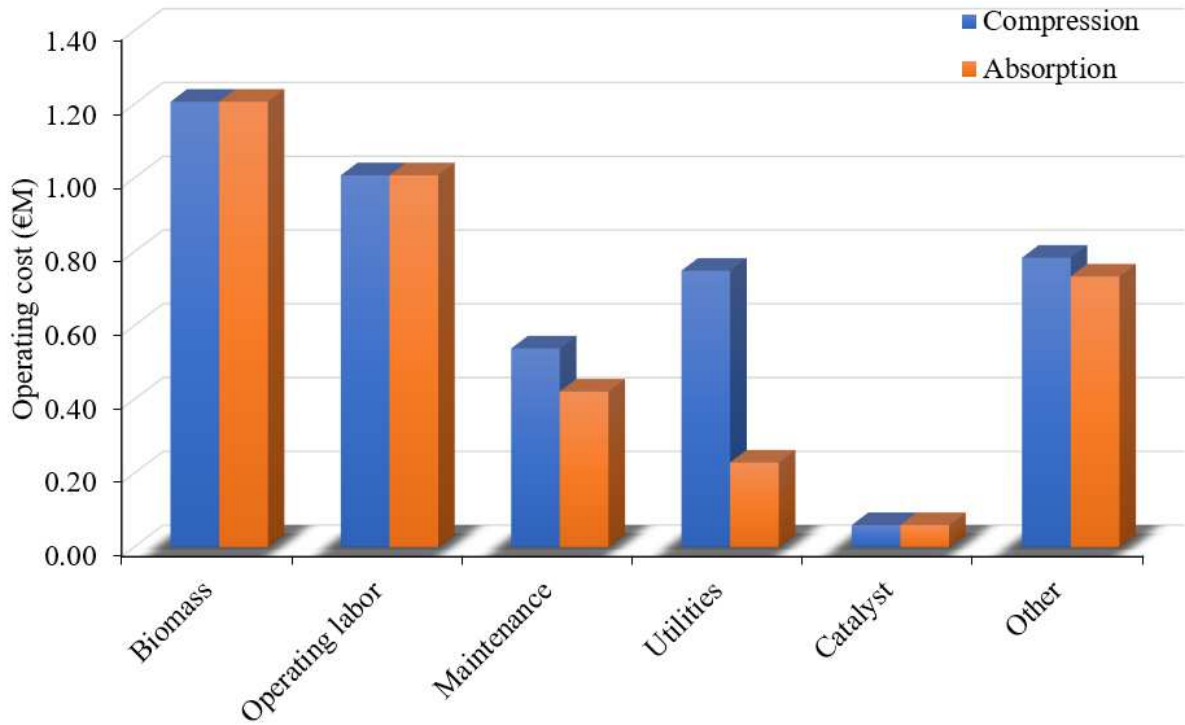
645



646

647 **Figure 22.** Total capital investment proportions for both schemes

648 The total operating costs of scheme-1 and scheme-2 were estimated at €4.9 million and €3.6  
649 million respectively. Figure 23 depicts the allocation of the two designs' constituent operating  
650 costs. The higher operating cost in scheme-1 compared to scheme-2 is due to the compression  
651 refrigeration machine's comparatively higher electricity usage. Table 13 states the cash flow  
652 of the process.



653

654

**Figure 23.** Operating cost proportions

655

656 **Table 13.** Cash flow of the process.

Item	Unit	Value
Number of Weeks per Period	Weeks/period	46.8
Number of Periods for Analysis	Period	20
Base year		2018
Duration of EPC Phase	Period	0.40
Duration of EPC Phase and Startup	Period	2.40
Working Capital Percentage	Percent/period	5
Operating Charges	Percent/period	25
Plant Overhead	Percent/period	50
Total Project Cost	Cost	1.79E+07
Total Raw Material Cost	Cost/period	1.21E+06
Total Operating Labor and Maintenance Cost	Cost/period	9.85E+05
Total Utilities Cost	Cost/period	674,706
Desired Rate of Return/Interest Rate	Percent/period	20

ROR Annuity Factor		5
Tax Rate	Percent/period	40
ROR Interest Factor		1.2
Economic Life of Project	Period	20
Salvage Value (Percent of Initial Capital Cost)	Percent	20
Depreciation Method		Straight Line
Project Capital Escalation	Percent/period	5
Products Escalation	Percent/period	5
Raw Material Escalation	Percent/period	3.5
Operating and Maintenance Labor Escalation	Percent/period	3
Utilities Escalation	Percent/period	3
Start Period for Plant Startup	Period	1
Desired Return on Project for Sales Forecasting	Percent/period	10.5
End Period for Economic Life of Project	Period	20
General and administrative Expenses	Percent/period	8
Duration of EP Phase before Start of Construction	Period	0.19
Total Operating Labor Cost	Cost/period	9.07E+05
Total Maintenance Cost	Cost/period	78,203

---

657

658 *3.2.3- Sensitivity analysis*

659       The impact of 30% difference in parameters listed in Table 8 was analyzed on the  
660 MFSPs of the two process schemes. The effect of variations in these parameters on the MFSP  
661 of scheme-1 and scheme-2 can be seen in the sensitivity charts in Figs. 24 and 25. The grey  
662 bars depict how sensitive base MFSPs are to a 30% rise in the parameters, while the blue bars  
663 portray how sensitive the base MFSPs are to a 30% decrease in the parameters. In general, the  
664 longer the bars, the more sensitive the base MFSPs are to parameter changes, and vice versa.  
665 Due to the marginal disparity in their capital and operational costs, and similarly in fuel

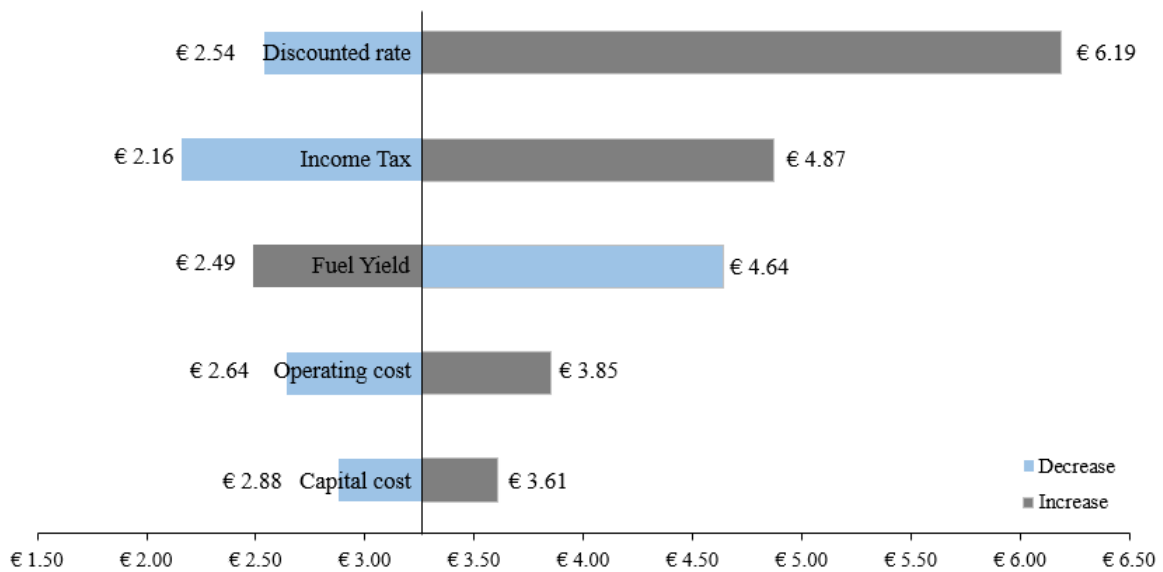
666 yields, the MFSPs of both process schemes display equal sensitivities to parameter variations,  
667 as seen in Figs. 24 and 25.

668 A 30% reduction in fuel yield resulted in a 42% increase in MFSP for scheme-1 and a  
669 39% increase in MFSP for scheme-2 (scheme-1: €4.64; scheme-2: €3.81). In contrast, a 30%  
670 rise in fuel yield resulted in a 23% decrease in MFSP for scheme-1 and a 21% decrease in  
671 MFSP for scheme-2 (scheme-1: €2.49; scheme-2: €2.05). This means that yield losses, which  
672 can occur as a result of events like operating and servicing issues, will hurt the profitability of  
673 both process schemes.

674 Scaling up the plant capacity, on the other hand, would be more commercially profitable  
675 for both process schemes. Increased plant capacity is one way to increase fuel yield, but it will  
676 give rise in capital and operating costs. Both designs' MFSPs were also moderately sensitive to  
677 changes in their operating costs. A 30% rise in operating costs resulted in a 18% increase in the  
678 MFSP for scheme-1 and a 16% increase in the MFSP for scheme-2 (scheme-1: €3.85; scheme-  
679 2: €3.18). In contrast, a 30% reduction in operating costs resulted in MFSP reductions of 19%  
680 for scheme-1 and 21% for scheme-2 (scheme-1: €2.64; scheme-2: €2.16). Since biomass feed  
681 costs account for a large portion of the running expense, as seen in Fig. 23, finding a less  
682 expensive option would be a safer economic decision. Variations in income tax had a major  
683 impact on the profitability of both method schemes.

684 A 30% rise in income tax resulted in a 49% and 46% increase in MFSPs of scheme-1  
685 and scheme-2 respectively (scheme-1: €4.87; scheme-2: €4.01), while a 30% decline in income  
686 tax resulted in 33% and 23% decrease in MFSPs of scheme-1 and scheme-2 respectively  
687 (scheme-1: €2.16; scheme-2: €1.78). This means that income tax reductions or deductions  
688 would be beneficial to the two operation schemes' profitability. As compared to the parameters  
689 discussed above, the MFSPs demonstrated less exposure to capital cost, with a 30% rise in  
690 capital cost triggering a 11% increase in scheme-1 and an 8% increase in scheme-2 (scheme-1:

691 €3.61; scheme-2: €2.96), and vice versa (scheme-1: €2.88; scheme-2: €2.38). The small impact  
 692 of higher capital investment on MFSPs, compared to the strong impact of higher bio-oil yield,

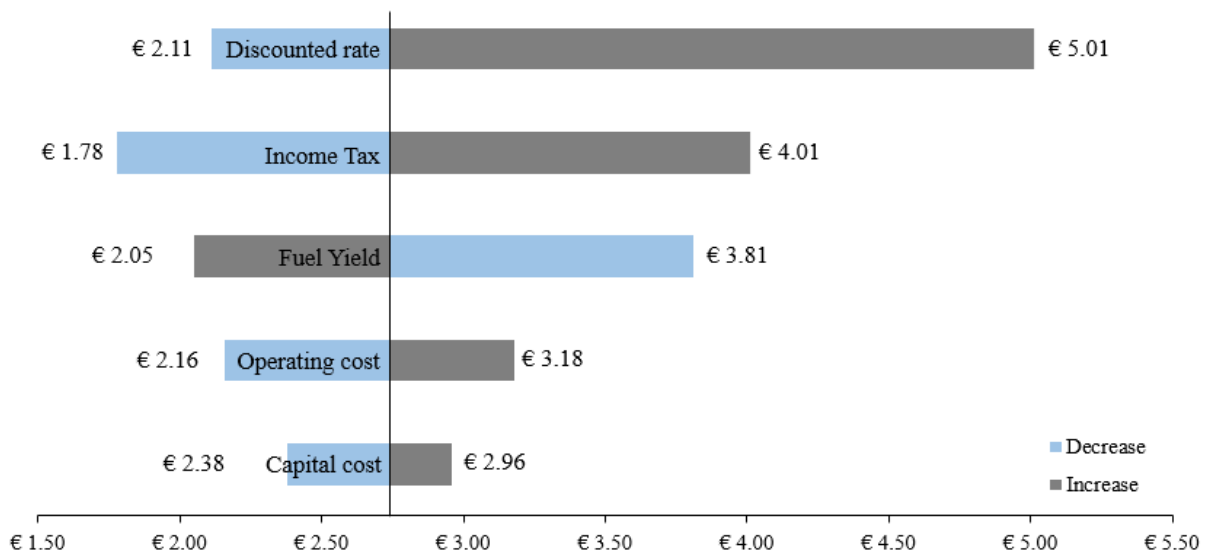


693 indicates that the profitability could be scaled up by increasing plant capacity.

694

695 **Figure 24.** Sensitivity analysis of MFSP

696



697

698 **Figure 25.** Scheme-2: Sensitivity of MFSP

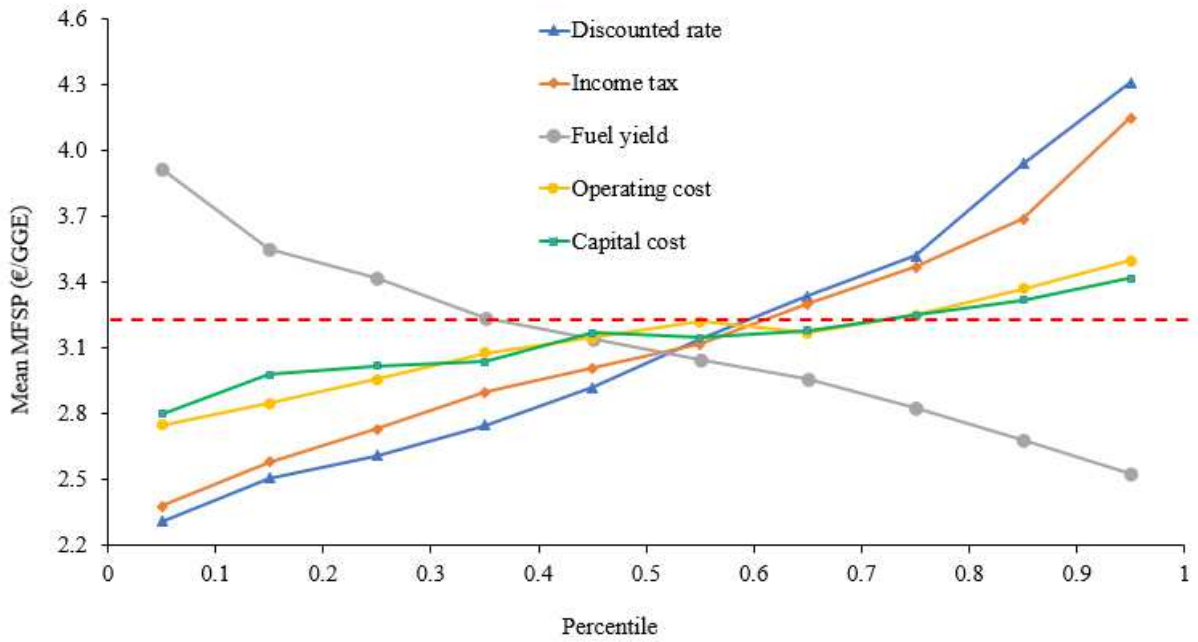
699 The above sensitivity analysis considered only single point variation of a parameters  
 700 on MFSP while other parameters were kept constant. To understand the variation of more



701 than one parameter at a time, a Monte Carlo sensitivity analysis was performed using  
702 ModelRisk software [54]. In the Figures 26 and 27, a spider chart has been created to analyze  
703 the sensitivity of the mean of the MFSP. Spider plots describe how sensitive the value of an  
704 output variable is to the input variable of the model. The horizontal axis shows the cumulative  
705 percentile of the economic parameters and the vertical axis shows the mean for the MFSP if  
706 the studied economic parameter value was around the percentile value of the horizontal axis.  
707 The horizontal line in the middle marks the mean MFSP. The precision of the percentile  
708 depends upon the number of tranches; in this case it is 10. This plot is generated using 10,000  
709 samples so each mean MFSP is calculated from 1,000 samples. Spider plot gives more  
710 information about the nature of the relationship between economic variables and MFSP. From  
711 the charts, it can be observed that capital cost and operating cost remain close to the mean  
712 MFSP line so they are least sensitive to MFSP. On the other hand, discounted rate and income  
713 tax cover the largest vertical range indicating that they are the most crucial parameters to be  
714 observed. Fuel yield has the similar relationship with MSFP but has slightly less influence.  
715 The mean MFSP is calculated to be €3.84/GGE for scheme-1 and €3.17/GGE for scheme-2.  
716 As discounted rate and income tax are more likely to remain constant during the life of the

717 plant, so increasing the fuel yield can bring down the MFSP of bio-oil significantly.

718 **Figure 26.** Spider chart for scheme-1



719

720

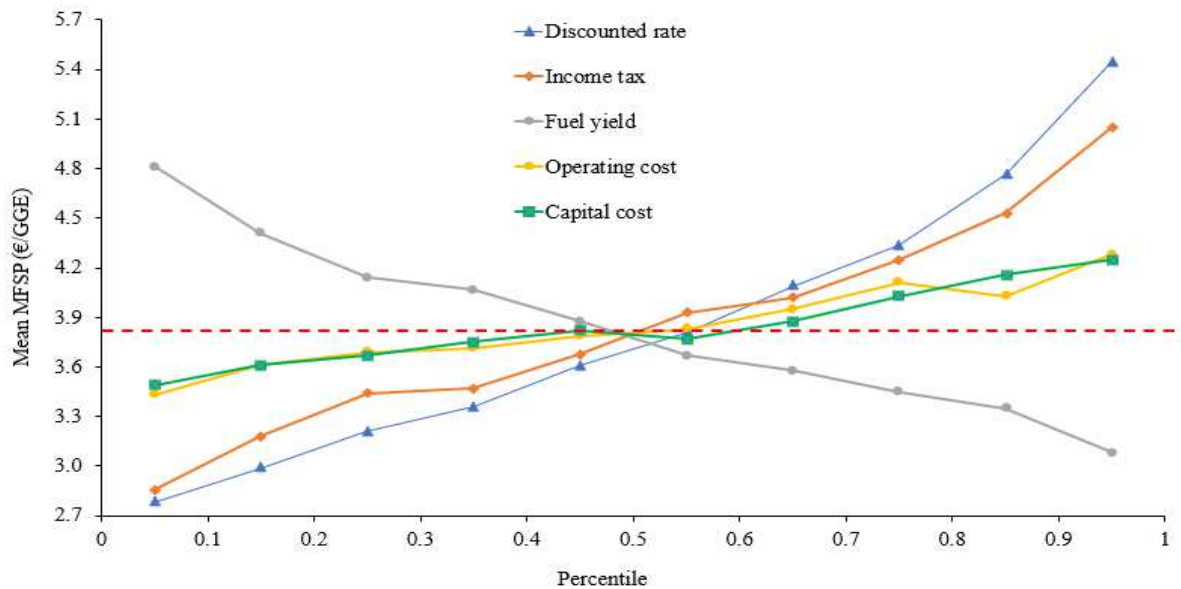
**Figure 27.** Spider chart for scheme-2

721

#### 722 4- Conclusion

723 A steady state model of pyrolysis of OMWS is developed in Aspen Plus under

724 standard pyrolysis conditions. A global reaction with kinetic parameters is employed in an



725 external Fortran user-subroutine and coupled with RCSTR reactor. For both catalytic and non-

726 catalytic pyrolysis, a good agreement between simulation and experimental yields can be  
727 observed.

728 For non-catalytic pyrolysis, maximum bio-oil yield is obtained at 450°C. Further  
729 increase in temperature favors the production of gas and char due to secondary cracking  
730 reaction in bio oil vapors thus decreasing the bio-oil yield at higher temperature. Simulation  
731 model depicts higher weight percentages of individual bio-oil components to accommodate  
732 the unknown compounds present in the bio-oil in experimental data. The prominent gas is  
733 CO<sub>2</sub> in the gaseous products comprising of about 81% at 400°C which decreases with rise in  
734 temperature. This decrease can be attributed to conversion of CO<sub>2</sub> into CO. Global absolute  
735 average deviation of 2.78% is observed for non-catalytic pyrolysis.

736 In the case of catalytic pyrolysis, the optimal temperature for bio-oil production is  
737 400°C at which bio-oil is about 34 wt.%. With rise in temperature, decline in bio-oil yield is  
738 observed. After 450°C, there is not a significant decrease in bio-oil yield, but gas quantity  
739 rises to 38 wt.% which can be regarded to decrease in char yield. For bio-oil, about 31%  
740 compounds are unknown in the experimental data so they are compensated with increased  
741 contribution from known compounds. Overall AAD for catalytic pyrolysis is about 3.54%.

742 From a technical and economic standpoint, the production of bio-oil from fast pyrolysis  
743 of olive mill wastewater sludge has been investigated. In terms of energy consumption and  
744 MFSP/GGE, two process schemes (scheme-1 and scheme-2) were examined and compared.  
745 The MFSP for scheme-1 is €3.26/GGE, based on a capital investment of €22.1 million and  
746 operational expenses of €4.6 million. Scheme-2, on the other hand, had a capital cost of €17.5  
747 million and an operating cost of €3.6 million. Scheme-2 had a 0.7 percent higher energy  
748 efficiency and a better economic performance than Scheme-1, with a MFSP of €2.74/GGE.  
749 Changes in bio-oil yield, operational expenses, and income tax were all equally sensitive to  
750 the MFSPs of scheme-1 and scheme-2. According to Monte Carlo sensitivity analysis,

751 increasing the bio-oil yield could bring the MFSP lower despite increase in capital and  
752 operating costs. The profitabilities can be improved considerably with reduction in income tax  
753 or exemptions.

## 754 **Acknowledgments**

755 The authors thank the financial supporters of the Waste2Fuel-ERANETMED2-72-298  
756 collaborative Euro-Mediterranean project. The Tunisian Ministry of Higher Education and  
757 Scientific Research, as well as the ANR in France, provided financial and administrative  
758 support to the writers. This work is also financed and carried out as a result of international  
759 collaboration between University of Lorraine, France and University of Sfax, Tunisia under  
760 the mechanism of DrEAM within the framework of Lorraine University of Excellence  
761 Initiative (LUE).

762

## 763 **References**

- 764 [1] P. Paraskeva, E. Diamadopoulos, Technologies for olive mill wastewater (OMW)  
765 treatment: A review, *J. Chem. Technol. Biotechnol.* (2006).  
766 <https://doi.org/10.1002/jctb.1553>.
- 767 [2] N. Sadhwani, S. Adhikari, M.R. Eden, P. Li, Aspen plus simulation to predict steady  
768 state performance of biomass-CO<sub>2</sub> gasification in a fluidized bed gasifier, *Biofuels,*  
769 *Bioprod. Biorefining.* (2018). <https://doi.org/10.1002/bbb.1846>.
- 770 [3] A. V. Bridgwater, Review of fast pyrolysis of biomass and product upgrading, *Biomass*  
771 *and Bioenergy.* (2012). <https://doi.org/10.1016/j.biombioe.2011.01.048>.
- 772 [4] M. Ling, M.J. Esfahani, H. Akbari, A. Foroughi, Effects of residence time and heating  
773 rate on gasification of petroleum residue, *Pet. Sci. Technol.* 34 (2016) 1837–1840.  
774 <https://doi.org/10.1080/10916466.2016.1230752>.
- 775 [5] S. Michailos, Kinetic modelling and dynamic sensitivity analysis of a fast pyrolysis  
776 fluidised bed reactor for bagasse exploitation, *Biofuels.* (2018) 1–10.  
777 <https://doi.org/10.1080/17597269.2018.1461522>.
- 778 [6] M.I. Jahirul, M.G. Rasul, A.A. Chowdhury, N. Ashwath, Biofuels production through  
779 biomass pyrolysis- A technological review, *Energies.* 5 (2012) 4952–5001.  
780 <https://doi.org/10.3390/en5124952>.
- 781 [7] M. Ouadi, J. Brammer, Y. Yang, A.H.-... and applied Pyrolysis, U. 2013, The  
782 intermediate pyrolysis of de-inking sludge to produce a sustainable liquid fuel, *J. Anal.*  
783 *Appl. Pyrolysis.* 102 (2013). <https://doi.org/https://doi.org/10.1016/j.jaap.2013.04.007>.

- 784 [8] S. Elkhalfa, A. AlNouss, T. Al-Ansari, H.R. Mackey, P. Parthasarathy, G. Mckay,  
785 Simulation of Food Waste Pyrolysis for the Production of Biochar: A Qatar Case  
786 Study, in: *Comput. Aided Chem. Eng.*, Elsevier B.V., 2019: pp. 901–906.  
787 <https://doi.org/10.1016/B978-0-12-818634-3.50151-X>.
- 788 [9] A. Dutta, A.H. Sahir, E. Tan, D. Humbird, L.J. Snowden-Swan, P.A. Meyer, J. Ross,  
789 D. Sexton, R. Yap, J. Lukas, *Process Design and Economics for the Conversion of*  
790 *Lignocellulosic Biomass to Hydrocarbon Fuels: Thermochemical Research Pathways*  
791 *with In Situ and Ex Situ Upgrading of Fast Pyrolysis Vapors*, Richland, WA (United  
792 States), 2015. <https://doi.org/10.2172/1238302>.
- 793 [10] A. AlNouss, G. Mckay, T. Al-Ansari, Optimum Utilization of Biomass for the  
794 Production of Power and Fuels using Gasification, in: *Comput. Aided Chem. Eng.*,  
795 Elsevier B.V., 2018: pp. 1481–1486. [https://doi.org/10.1016/B978-0-444-64235-](https://doi.org/10.1016/B978-0-444-64235-6.50258-8)  
796 [6.50258-8](https://doi.org/10.1016/B978-0-444-64235-6.50258-8).
- 797 [11] S. Elkhalfa, A. AlNouss, T. Al-Ansari, ... H.M.-C.A., undefined 2019, Simulation of  
798 Food waste pyrolysis for the production of biochar: a qatar case study, Elsevier. (n.d.).  
799 <https://www.sciencedirect.com/science/article/pii/B978012818634350151X> (accessed  
800 June 12, 2021).
- 801 [12] I.A. Vasalos, A.A. Lappas, E.P. Kopalidou, K.G. Kalogiannis, Biomass catalytic  
802 pyrolysis: process design and economic analysis, *Wiley Interdiscip. Rev. Energy*  
803 *Environ.* 5 (2016) 370–383. <https://doi.org/10.1002/wene.192>.
- 804 [13] J.Y. Park, J.K. Kim, C.H. Oh, J.W. Park, E.E. Kwon, Production of bio-oil from fast  
805 pyrolysis of biomass using a pilot-scale circulating fluidized bed reactor and its  
806 characterization, *J. Environ. Manage.* 234 (2019) 138–144.  
807 <https://doi.org/10.1016/j.jenvman.2018.12.104>.
- 808 [14] J.F. Peters, S.W. Banks, A. V. Bridgwater, J. Dufour, A kinetic reaction model for  
809 biomass pyrolysis processes in Aspen Plus, *Appl. Energy.* 188 (2017) 595–603.  
810 <https://doi.org/10.1016/j.apenergy.2016.12.030>.
- 811 [15] I.Y. Mohammed, Y.A. Abakr, R. Mokaya, Integrated biomass thermochemical  
812 conversion for clean energy production: Process design and economic analysis, *J.*  
813 *Environ. Chem. Eng.* 7 (2019). <https://doi.org/10.1016/j.jece.2019.103093>.
- 814 [16] M.B. Shemfe, S. Gu, P. Ranganathan, Techno-economic performance analysis of  
815 biofuel production and miniature electric power generation from biomass fast pyrolysis  
816 and bio-oil upgrading, *Fuel.* 143 (2015) 361–372.  
817 <https://doi.org/10.1016/j.fuel.2014.11.078>.
- 818 [17] K. Onarheim, Y. Solantausta, J. Lehto, Process simulation development of fast  
819 pyrolysis of wood using aspen plus, *Energy and Fuels.* 29 (2015) 205–217.  
820 <https://doi.org/10.1021/ef502023y>.
- 821 [18] J.F. Peters, F. Petrakopoulou, J. Dufour, Exergetic analysis of a fast pyrolysis process  
822 for bio-oil production, *Fuel Process. Technol.* 119 (2014) 245–255.  
823 <https://doi.org/10.1016/j.fuproc.2013.11.007>.
- 824 [19] M. Patel, A.O. Oyedun, A. Kumar, R. Gupta, What is the production cost of renewable  
825 diesel from woody biomass and agricultural residue based on experimentation? A  
826 comparative assessment, *Fuel Process. Technol.* 191 (2019) 79–92.  
827 <https://doi.org/10.1016/j.fuproc.2019.03.026>.

- 828 [20] M. Patel, A.O. Oyedun, A. Kumar, R. Gupta, What is the production cost of renewable  
829 diesel from woody biomass and agricultural residue based on experimentation? A  
830 comparative assessment, *Fuel Process. Technol.* 191 (2019) 79–92.  
831 <https://doi.org/10.1016/j.fuproc.2019.03.026>.
- 832 [21] E. Ranzi, A. Cuoci, T. Faravelli, A. Frassoldati, G. Migliavacca, S. Pierucci, S.  
833 Sommariva, Chemical kinetics of biomass pyrolysis, *Energy and Fuels*. 22 (2008)  
834 4292–4300. <https://doi.org/10.1021/ef800551t>.
- 835 [22] A. Khosravanipour Mostafazadeh, O. Solomatnikova, P. Drogui, R.D. Tyagi, A review  
836 of recent research and developments in fast pyrolysis and bio-oil upgrading, *Biomass*  
837 *Convers. Biorefinery*. 8 (2018) 739–773. <https://doi.org/10.1007/S13399-018-0320-Z>.
- 838 [23] Y. Zeng, B. Zhao, L. Zhu, D. Tong, C.H.-R. Advances, U. 2013, Catalytic pyrolysis of  
839 natural algae from water blooms over nickel phosphide for high quality bio-oil  
840 production, *RSC Adv.* (2013).
- 841 [24] T. Aysu, A. Sanna, Nannochloropsis algae pyrolysis with ceria-based catalysts for  
842 production of high-quality bio-oils, *Bioresour. Technol.* 194 (2015) 108–116.  
843 <https://doi.org/10.1016/J.BIORTECH.2015.07.027>.
- 844 [25] Y. Yang, J.G. Brammer, M. Ouadi, J. Samanya, A. Hornung, H.M. Xu, Y. Li,  
845 Characterisation of waste derived intermediate pyrolysis oils for use as diesel engine  
846 fuels, *Fuel*. 103 (2013) 247–257. <https://doi.org/10.1016/J.FUEL.2012.07.014>.
- 847 [26] M. Tripathi, J.N. Sahu, P. Ganesan, Effect of process parameters on production of  
848 biochar from biomass waste through pyrolysis: A review, *Renew. Sustain. Energy Rev.*  
849 55 (2016) 467–481. <https://doi.org/10.1016/J.RSER.2015.10.122>.
- 850 [27] J. Alvarez, M. Amutio, G. Lopez, J. Bilbao, M. Olazar, Fast co-pyrolysis of sewage  
851 sludge and lignocellulosic biomass in a conical spouted bed reactor, *Fuel*. 159 (2015)  
852 810–818. <https://doi.org/10.1016/J.FUEL.2015.07.039>.
- 853 [28] V. Anand, V. Sunjeev, R. Vinu, Catalytic fast pyrolysis of *Arthrospira platensis*  
854 (*spirulina*) algae using zeolites, *J. Anal. Appl. Pyrolysis*. 118 (2016) 298–307.  
855 <https://doi.org/10.1016/J.JAAP.2016.02.013>.
- 856 [29] Q. Xu, X. Ma, Z. Yu, Z. Cai, A kinetic study on the effects of alkaline earth and alkali  
857 metal compounds for catalytic pyrolysis of microalgae using thermogravimetry, *Appl.*  
858 *Therm. Eng.* 73 (2014) 357–361.  
859 <https://doi.org/10.1016/J.APPLTHERMALENG.2014.07.068>.
- 860 [30] X. Dong, Z. Chen, S. Xue, J. Zhang, J. Zhou, Y. Liu, ... Y.X.-R., U. 2013, Catalytic  
861 pyrolysis of microalga *Chlorella pyrenoidosa* for production of ethylene, propylene and  
862 butene, *RSC Adv.* (2013).
- 863 [31] M.N. Islam, F.N. Ani, Techno-economics of rice husk pyrolysis, conversion with  
864 catalytic treatment to produce liquid fuel, *Bioresour. Technol.* 73 (2000) 67–75.  
865 [https://doi.org/10.1016/S0960-8524\(99\)00085-1](https://doi.org/10.1016/S0960-8524(99)00085-1).
- 866 [32] M. Shemfe, S. Gu, B. Fidalgo, Techno-economic analysis of biofuel production via  
867 bio-oil zeolite upgrading: An evaluation of two catalyst regeneration systems, *Biomass*  
868 *and Bioenergy*. 98 (2017) 182–193. <https://doi.org/10.1016/j.biombioe.2017.01.020>.
- 869 [33] M.M. Wright, D.E. Daugaard, J.A. Satrio, R.C. Brown, Techno-economic analysis of  
870 biomass fast pyrolysis to transportation fuels, *Fuel*. 89 (2010) S2–S10.

- 871 <https://doi.org/10.1016/j.fuel.2010.07.029>.
- 872 [34] A. Dutta, J.A. Schaidle, D. Humbird, F.G. Baddour, A. Sahir, Conceptual Process  
873 Design and Techno-Economic Assessment of Ex Situ Catalytic Fast Pyrolysis of  
874 Biomass: A Fixed Bed Reactor Implementation Scenario for Future Feasibility, *Top.*  
875 *Catal.* 59 (2016) 2–18. <https://doi.org/10.1007/s11244-015-0500-z>.
- 876 [35] F. Aryi Agblevor, H. Abdellaoui, K. Halouani, S. Hakis Beis, Pyrolytic Conversion of  
877 Olive Mill Wastewater Sludge to Biofuels Using Red Mud as Catalyst, *Int. J. Energy*  
878 *Power Eng.* 6 (2017) 108. <https://doi.org/10.11648/j.ijepe.20170606.14>.
- 879 [36] AspenTech, Aspen Plus user models, (n.d.). <https://www.aspentech.com/en>.
- 880 [37] A.G. Adeniyi, J.O. Ighalo, M.K. Amosa, Modelling and simulation of banana (*Musa*  
881 *spp.*) waste pyrolysis for bio-oil production, *Biofuels.* (2019).  
882 <https://doi.org/10.1080/17597269.2018.1554949>.
- 883 [38] J. Ward, M.G. Rasul, M.M.K. Bhuiya, Energy recovery from biomass by fast pyrolysis,  
884 in: *Procedia Eng.*, Elsevier Ltd, 2014: pp. 669–674.  
885 <https://doi.org/10.1016/j.proeng.2014.11.791>.
- 886 [39] J.F. Peters, D. Iribarren, J. Dufour, Predictive pyrolysis process modelling in Aspen  
887 Plus ®, in: *Researchgate.Net*, Copenhagen, 2014.  
888 <https://doi.org/10.5071/21stEUBCE2013-2CV.4.8>.
- 889 [40] N. Gautam, A. Chaurasia, Study on kinetics and bio-oil production from rice husk, rice  
890 straw, bamboo, sugarcane bagasse and neem bark in a fixed-bed pyrolysis process,  
891 *Energy.* 190 (2020) 116434. <https://doi.org/10.1016/j.energy.2019.116434>.
- 892 [41] A.T. Talwalkar, IGT/DOE coal-conversion systems technical data book, 1981.
- 893 [42] R.L. Diaz, J C; Braun, Process simulation model for a staged, fluidized-bed oil-shale  
894 retort with lift-pipe combustor (Technical Report) | OSTI.GOV, 1984.
- 895 [43] AspenTech, Aspen Plus model for oil shale retorting process, (2010).
- 896 [44] C. Somers, A. Mortazavi, Y. Hwang, R. Radermacher, P. Rodgers, S. Al-Hashimi,  
897 Modeling water/lithium bromide absorption chillers in ASPEN Plus, *Appl. Energy.* 88  
898 (2011) 4197–4205. <https://doi.org/10.1016/j.apenergy.2011.05.018>.
- 899 [45] R. Reid, J. Prausnitz, B. Poling, *The properties of gases and liquids*, (1987).  
900 <https://www.osti.gov/biblio/6504847> (accessed May 27, 2021).
- 901 [46] ASHRAE, *Handbook-fundamentals*, 1997.
- 902 [47] N. Grioui, K. Halouani, A. Zoulalian, F. Halouani, Thermochemical modeling of  
903 isothermal carbonization of thick wood particle - Effect of reactor temperature and  
904 wood particle size, *Energy Convers. Manag.* 48 (2007) 927–936.  
905 <https://doi.org/10.1016/j.enconman.2006.08.003>.
- 906 [48] Cost Indices, (n.d.). <https://www.toweringskills.com/financial-analysis/cost-indices/>.
- 907 [49] France electricity prices, September 2020 | *GlobalPetrolPrices.com*, (n.d.).  
908 [https://www.globalpetrolprices.com/France/electricity\\_prices/](https://www.globalpetrolprices.com/France/electricity_prices/) (accessed April 26,  
909 2021).
- 910 [50] TUNISIA - 2021 Finance Law - BDO, (n.d.). <https://www.bdo.global/en->

- 911 gb/microsites/tax-newsletters/corporate-tax-news/issue-58-april-2021/tunisia-2021-  
912 finance-law.
- 913 [51] R.E.W. Max S. Peters, Klaus D. Timmerhaus, Plant design and economics for chemical  
914 engineers, 5th ed., McGraw-Hill, 2003.
- 915 [52] A. Pattiya, J.O. Titiloye, A. V. Bridgwater, Evaluation of catalytic pyrolysis of cassava  
916 rhizome by principal component analysis, *Fuel*. 89 (2010) 244–253.  
917 <https://doi.org/10.1016/j.fuel.2009.07.003>.
- 918 [53] F. Paviet, F. Chazarenc, M. Tazerout, Thermo chemical equilibrium modelling of a  
919 biomass gasifying process using ASPEN pLUS, *Int. J. Chem. React. Eng.* 7 (2009).  
920 <https://doi.org/10.2202/1542-6580.2089>.
- 921 [54] Risk Analysis Software for Excel | Vose Software, (n.d.).  
922 <https://www.vosesoftware.com/products/modelrisk/>.
- 923